Physics – Uspekhi **63** (10) 994 – 1014 (2020)

REVIEWS OF TOPICAL PROBLEMS

PACS numbers: **71.30.+h, 72.10.–d**, 72.15.Rn, 72.20.Ee, 72.80.Ng, 73.21.La, **73.22.–f**, 73.23.Hk, 73.40.Gk, 81.07.Bc

Conductivity of quantum dot arrays

K V Reich

DOI: https://doi.org/10.3367/UFNe.2019.08.038649

Contents

1. Introduction **994**
2. Producing a quantum dot array **996**
3. Model and main parameters of a quantum dot **997**
3.1 Kinetic energy; 3.2 Electrostatic energy; 3.3 Model applicability conditions
4. Array of quantum dots **999**
4.1 Dielectric constant; 4.2 Overlap integral; 4.3 Disorder in a QD array; 4.4 Density of states; 4.5 Localization length
5. Metal–insulator transition **1005**
5.1 Geometric disorder in a QD array; 5.2 Doped QD array
6. Insulating phase **1007**
6.1 Temperature dependence of conductivity; 6.2 Doped QD arrays; 6.3 Charge distribution in a field transistor; 6.4 Disorder in sizes and in distances between QDs; 6.5 Conductivity in a field transistor; 6.6 Doping from the surface
7. Conclusions **1012**
References **1013**

Abstract. Arrays of quantum dots (QDs), i.e., semiconducting nanoparticles with typical sizes of 3–10 nm, have become more than merely an object of scientific research; they are now used in electronic devices. They are appealing mainly due to their optical properties, which depend on the QD size. Here, we consider the electronic properties of such arrays. These properties typically inherit the properties of bulk semiconductors, but in some cases can be substantially different due to the discreteness of sizes and a particular type of disorder in the array: the difference in size and spacing among QDs, as well as the number of donors. Notably, in such arrays, the metal–dielectric transition occurs at a much higher concentration of donors than in the bulk material. The nature of hopping conductivity in the dielectric phase strongly depends on the disorder type, quantum confinement effects, the Coulomb blockade, and the overlap integral of QDs.

Keywords: quantum dot, nanoparticle, quantum confinement, electron transport, metal–insulator transition, Coulomb interaction, Coulomb blockade

1. Introduction

This review is devoted to a discussion of modern approaches to describing the conductivity of arrays of quantum dots (QDs) — semiconducting nanoparticles with typical sizes D less than 10 nm.

K V Reich Ioffe Institute,
ul. Politekhnicheskaya 26, 194021 St. Petersburg, Russian Federation
E-mail: Reich@mail.ioffe.ru

Received 4 July 2019, revised 25 August 2019
Uspekhi Fizicheskikh Nauk **190** (10) 1062 – 1084 (2020)
Translated by S Alekseev

In recent decades, the continuing interest in these objects is motivated by the possibility of varying the optical properties of QDs by changing their size, as well as by the technological ease of their industrial production [1]. Just the spectral dependence of optical absorption on the QD size initially triggered the start of investigations of these objects. This dependence has been demonstrated for various semiconducting materials, including in silicon QDs [2].

Quantum dots made their appearance more than 40 years ago, when their optical properties were for the first time described experimentally [3, 4]. A theoretical explanation of the observed optical effects followed almost immediately [5]. Today, despite the many years of investigations and the results achieved, this area of physics is blossoming. New areas for QD applications are solar panels [6], LEDs [7, 8], biomarkers [9], and transmitters and receivers of infrared radiation [10, 11]. Progress in studying the optical properties of QDs is described in a number of reviews [9, 12–14]. We also note that displays based on QDs have outgrown the development stage [15] and are now produced by Samsung (South Korea).

At the same time, in many applications in optoelectronic devices, not only the optical properties but also the electric conductivity of QD arrays is essential. In particular, the efficiency factor of QD-based solar elements is limited by the mobility of holes and electrons [16]. But the electric conductivity of QD arrays is studied much less.

In analyzing the optical properties, we can safely restrict ourselves to considering a single QD, but describing the electronic properties requires considering collections — arrays — of QDs. From the physical standpoint, this is the current problem to be investigated about the conductivity of QD arrays.

We note that the electronic properties of individual nanoparticles have been broadly studied over the last 20 years. It was shown, for example, that the principal

element of electron transport through a nanoparticle is the Coulomb blockade [17]. This classic effect refers to the simple fact that an additional electron can only be added to a nanoparticle if its energy suffices for overcoming the Coulomb repulsion of other electrons. As a logical continuation, two nanoparticles were considered [18] and, eventually, an array of nanoparticles. An analysis of electron transport in an array of metallic nanoparticles is presented in reviews [19, 20]. In contrast to metallic nanoparticles, an essential role is played in an array of semiconducting QDs by the quantum confinement effect, entailing quantization of the kinetic energy of electrons in such QDs. The quantization energy can be much higher than the Coulomb blockade energy. In addition, the number of electrons in such QDs can vary in a broad range and reach 50 electrons per QD [21].

In what follows, we focus on the analysis of recent results obtained in investigating the conductivity of semiconducting QD arrays. We mainly consider theoretical results; experimental data are discussed in reviews [22–24].

We discuss here two types of QD arrays. The first is where the QDs are separated from each other by ligands that cover their surfaces (Fig. 1a). Obviously, increasing the conductivity of an array requires decreasing the distance s between QDs, i.e., decreasing the length of these ligands [25]. In the limit, the ligands can be eliminated and QDs can merge epitaxially so as to touch each other with their faces [26–28]. This leads us to the second case: arrays of QDs whose faces touch each other, the typical size of the face being $\rho \sim 1$ nm (Fig. 1b). It is obvious that increasing the contact area leads to an increase in the conductivity of the array, but suppresses its unique optical properties.

As in the case of a bulk semiconductor, changing the conducting properties requires introducing electrons into semiconducting QDs, which otherwise would be insulating. The doping of QDs is the main problem here [29], which was solved only very recently. This explains some difficulties in comparing the theory that has been developed and a limited amount of experimental data.

Several strategies have allowed inducing electrons into the conductivity band of QDs. First, the doping of QDs in a wide range of concentrations has become possible [21]. Second, electrons can be induced using the field effect, i.e., by creating a field transistor with QDs [30–32]. Third, sufficiently large numbers of electrons can be induced into a QD electrochemically, i.e., using an ionic liquid [33].

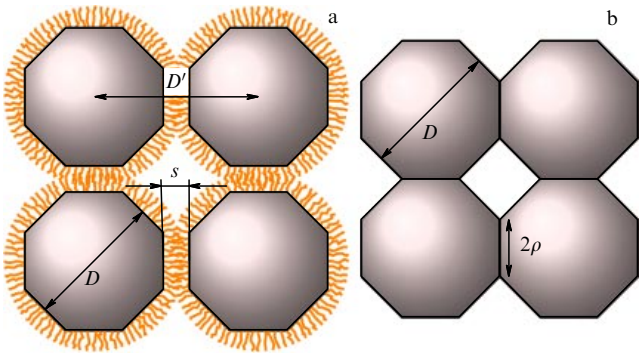

Figure 1. Outline of QD arrays. (a) Due to ligands, QDs with a typical size $D \sim 10$ nm are separated by a distance $s \sim 1$ nm, with the distance between QD centers $D' = D + s$. (b) QDs without ligands touch each other with their faces with typical size $\rho \sim 1$ nm.

In Section 2, the role of ligands, the difficulties encountered in doping QDs, and the methods for measuring the conductivity of arrays are discussed in more detail.

Evidently, the properties of a QD array are determined by the properties of individual QDs, and in Section 3 we therefore consider an isolated QD. From the standpoint of transport properties of a QD array, two energy values are important: the Coulomb energy E_C that is necessary for transferring one elementary charge onto a QD and which is related to the Coulomb blockade, and the kinetic energy quantum of the electron in such QDs, Δ. We mainly focus on the case where $\Delta \gg E_C$, because the properties of a QD array then differ greatly from the properties of an array of metallic QDs.

The parameters of an array can be strongly different from the parameters of a single QD. For instance, the permittivity κ_{QD} of a single QD can be much greater than the permittivity κ of the entire array. The most substantial, and fundamental, difference between an array and a single QD is the appearance of disorder. QDs can differ from each other in size, in the number of donors in each QD, and in the distance s between neighbors. The density of states $g(\varepsilon)$ in an array and the position of the Fermi level ε_F are therefore quite different from those for a single QD. Disorder typically leads to localization of electrons in QDs when the spread of energy levels in the system, γ, is greater than the overlap integral t of QDs. In Section 4, we discuss these parameters of QD arrays.

If $t \simeq \gamma$, a transition from the insulating to the metallic state occurs in a QD array. The possibility of such a transition is still being doubted by some researchers [34]. We consider conditions for this transition in the presence of disorder in size and distances between QDs, when electrons in the array are induced due to the field effect in a field transistor structure.

For doped QD arrays, these conditions change substantially, because an additional type of disorder appears, one related to variation in the number of donors from one QD to another. It is known that in a bulk semiconductor with a permittivity κ_{QD} and effective electron mass m, the transition occurs at the concentration of donors $na_B^3 = 0.02$ [35], where $a_B = \hbar^2\kappa_{QD}/me^2$ is the Bohr radius (here and hereafter, we use the CGS system of units). For doped QDs whose faces touch, with the donor concentration n, the insulator–metal transition can be observed at the critical size of the face ρ_c such that [21]

$$n\rho_c^3 \simeq 1\,. \tag{1}$$

It hence follows that, for $\rho_c \sim 1$ nm, the doping level must be enormous: $n \sim 10^{21}$ cm^{-3}. No such transition has been observed so far, but a characteristic scaling of conductivity is observed experimentally near the transition [36], which is similar to what is known for the bulk material. Details of the insulator–metal transition in an array of semiconducting crystals are discussed in Section 5 below.

Because of the Coulomb blockade effect, even the arrays of metallic nanoparticles are typically insulating: their conductivity G decreases exponentially with temperature T [37]. It is therefore unsurprising that, in most cases, the arrays of doped semiconducting QDs are insulating, their conductivity following the law

$$G \propto \exp\left(-\left(\frac{E_0}{kT}\right)^p\right), \tag{2}$$

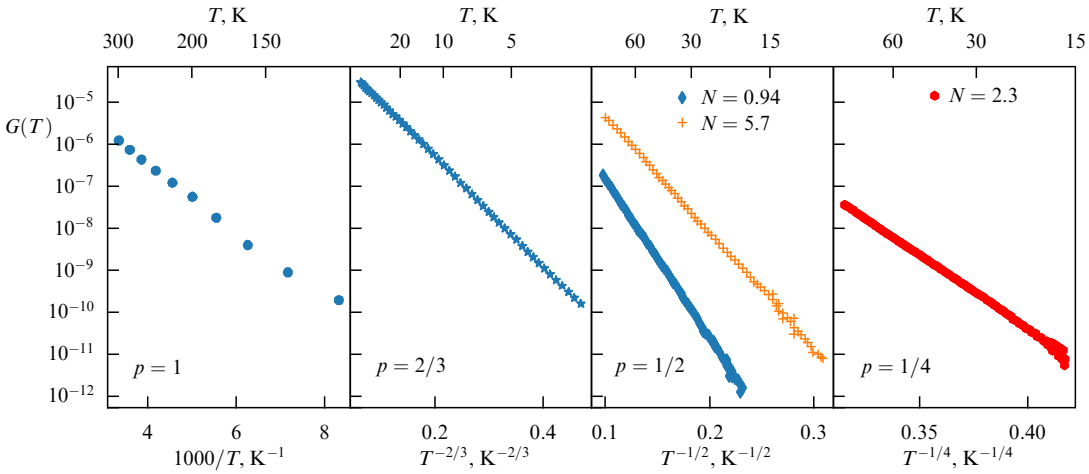

Figure 2. Examples of typical experimental dependences of the conductivity of a QD array on temperature $G(T)$. The data for an activation dependence with the exponent $p = 1$ are taken from [38], and for $p = 2/3$, from [39]. The ES dependence for $p = 1/2$ and the Mott dependence for $p = 1/4$ are taken from [40]. In all cases, the experimental data are rectified in the $\ln G$–T^{-p} coordinates.

where the coefficients E_0 and p are determined by the transport mechanism, which in turn depends on the parameters of the array and the temperature interval.

For example, in an array of doped QDs, the Efros–Shklovskii (ES) law with the power-law exponent $p = 1/2$ is typically observed at low temperatures, activation transport $p = 1$ sets in at high temperatures, and Mott transport $p = 1/4$, at intermediate temperatures (Fig. 2).

In a field transistor, the conductivity (and mobility) is also significantly dependent on the number of induced electrons. In such a device, we focus on how the electric conductivity depends on disorder in the distances between QDs. We discuss the features related to electrochemical doping. As in bulk semiconductors, this process is analogous to doping from the surface [41]. Interestingly, in the case of electrochemical doping, dependence (2) can be observed with the exponent $p = 2/3$ (see Fig. 2, the case $p = 2/3$), which defies a generally satisfactory explanation. These problems are discussed in Section 6 below.

In passing to the main contents of this review, we note that we are actually dealing with electron transport in QD arrays, but all our conclusions are also applicable to hole transport.

2. Producing a quantum dot array

The technology of growing QDs has been discussed in a number of reviews [22, 42–45]. In this section, we expound the principal theoretical concepts regarding the production of QD arrays and illustrate the difficulties in doping such materials and possible strategies to overcome these difficulties.

A major part of the QDs investigated today are obtained in the liquid phase from A_2B_6 and A_3B_5 compounds. As rule, the precursor (salt A) is rapidly introduced into a strongly heated solvent containing the B component. Subsequent cooling produces QDs [46]. Importantly, this process requires the presence of organic surface-active substances — ligands — in the solution, which attach to the growing QDs and prevent them from sintering. We emphasize that just the ligands govern the kinetics of QD growth. This technology is broadly developed and allows growing QDs of any shape and size [45]. In addition, ligands allow reducing the number of surface states in a QD, which are a hindrance to electron transport processes.

The drawbacks of this method stem from its advantages. On the one hand, the surface of obtained QDs is covered with ligands and, therefore, the distance s between adjacent QDs is sufficiently large, which, as noted above, hinders electron transport. This problem can be partially solved if, after the synthesis of QDs, the ligands are chemically replaced with shorter ones. This method leads to an increase in the conductivity of the system [22].

On the other hand, it is difficult to obtain strongly doped QDs with this method. At the synthesis temperature of about 300 °C, crystals undergo "self-cleaning" [29], with the impurities going out to the surface. This drawback can be partially overcome if the ligands on the surface are themselves donors [47, 48].

Several other approaches have been proposed to achieve higher degrees of QD doping in crystallization from the liquid phase [49]. However, it has so far been impossible to achieve a high degree of doping (a dozen donors per QD).

Yet another approach consists of producing QDs from the gas phase. This method assumes the use of low-temperature plasma [50]. Electrons in such plasma have a temperature of about 10^4 K, and collisions of electrons with molecules lead to effective dissociation and ionization of the precursor gas. The produced ions and radicals form nanoparticles. Although the electron temperature is high, the temperature of the resultant particles is sufficiently low. Adding a donor component to the gas phase allows attaining high donor concentrations in QDs, since the low temperature of QDs is insufficient for the diffusion of donors to the surface [51].

The high concentration of electrons in the bulk of QDs can be prevented by surface states, whose concentration in QDs is high [8]. Therefore, the average number of deep surface states, which can trap electrons from the conductivity band, must be much less than the average number of donors in a QD. Technologies are being developed with the aim to reduce the concentration of surface states. For instance, the use of inorganic ligands has allowed reducing the density of deep surface states by an order of magnitude, to 10^{10} cm^{-2} eV^{-1} [52, 53]. Progress in technology allows us to hope that this problem will be solved, and we do not consider

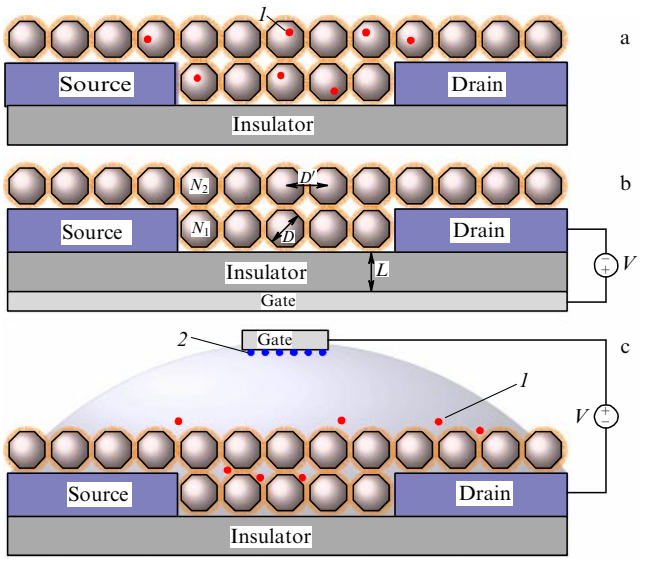

Figure 3. Different configurations of a QD array for conductivity measurements. In all three cases, the array is placed on a substrate with source and drain contacts. (a) Doped QD array. Red dots *1* show the donors. (b) Field transistor. Under a bias V, electrons accumulate in the first two QD layers closest to the gate. N_1 and N_2 are the average numbers of electrons in the first and the second layers. (c) Field transistor with an ionic liquid (electrolyte) used as the gate insulator. Under a bias V, negative ions drift toward the gate (blue dots *2*) and positive ions drift toward the QD array (red dots *1*), while electrons are induced in the QD array.

effects associated with surface states in the theoretical analysis in what follows.

The next stage in producing a QD array is the deposit of QDs onto a substrate. The array can then be ordered in several ways, and the same QDs can be arranged into one-dimensional, two-dimensional, or three-dimensional structures [54], depending on the conditions of deposition. Quantum dots covered with ligands can make up two-dimensional superlattices [44, 55], as outlined in Fig. 1a.

The main problem is to ensure the high conductivity of the resultant array as a whole. When QDs have regular faceting, one way to increase the conductivity is to remove ligands from the QD surface. This method for obtaining a "clean" surface of the faces and ensuring direct contact between faces of QDs allows creating superlattices of touching QDs [26, 56–58], as is outlined in Fig. 1b.

Evidently, obtaining an ordered lattice of QDs is a complicated technological problem. Typically, a random close packing is produced in depositing bulk arrays (films) of QDs [59].

In our theoretical calculations, in what follows, we assume that QDs are arranged into a cubic lattice; this greatly simplifies the mathematical derivations. But an important point is that changing the lattice type does not affect the derived conclusions and leads to only inessential changes in the coefficients in formulas.

The conductivity of a QD array can be measured in three different configurations.

For an array of doped QDs, the simplest configuration can be used (Fig. 3a): it suffices to place the array on a substrate and draw the source and drain contacts. We note that, as we show in what follows, doping a QD introduces unremovable disorder.

For a doped QD array, it is necessary to induce electrons, and this can be carried out using the field effect in a field transistor structure (Fig. 3b). Here, as we show in the following, electrons are induced only in the first two layers, the ones closest to the gate.

In both QD arrays and thin films [60], electrons can also be induced using an ionic liquid [33, 61], which consists of an equal number of positive (cations) and negative (anions) ions. As a bias V is applied to the gate (Fig. 3c) at room temperature, the anions drift toward the gate and the cations toward the QD array, penetrating into the depth of the array, which then neutralizes the induced electron charge in the array. We note that here we are speaking of only an inconsiderable proportion of additional ions near the surface, whereas in each domain inside the liquid on the whole, positive ions are balanced by negative ions. Electroconductivity is then measured at temperatures below room temperature, when the ionic liquid freezes and becomes nonconducting. Thus, the use of ionic liquid is, in effect, similar to doping from the surface [41]. The system involving ionic liquid as the insulator allows inducing many more electrons into the QD, which is an important advantage compared with the conventional field transistor structure. The ions, unlike donors, can be redistributed among the QDs, reducing the associated disorder.

3. Model and main parameters of a quantum dot

The band structure of a single nanoparticle inherits the properties of the band structure of the material it is made of and can be quite complicated. In particular, an important role can be played by spin–orbit and crystal-field splitting. Still, in contrast to optical effects, these factors have not so far been observed experimentally to affect electron transport. Therefore, in the theory expounded below, we consider only a simple parabolic model of the band structure of QDs.

In this section, we focus on a single QD and consider the main energy parameters of the model: the kinetic energy E_Q of the electron and the energy E_c necessary for adding one electron to a neutral QD, which is called the charging energy.

3.1 Kinetic energy

In the conductivity band of a QD, due to its small size, the possible values of the kinetic energy of electrons E_Q are quantized (Fig. 4).

In the model under consideration, we also assume that the QDs are spheres of diameter D, and the wave function on the QD surface is close to zero due to the large value of the work function φ.

Under the assumptions made in the simple band model, the kinetic energy of an Nth electron added to the QD can be written as

$$E_Q(N) = \frac{\hbar^2}{mD^2}\begin{cases} 0\,, & N = 0 \\ 19.74\,, & N = 1, 2 \quad (1s) \\ 40.38\,, & 3 \leqslant N \leqslant 8 \quad (1p) \\ \ldots\ldots \end{cases}. \qquad (3)$$

Hence, it follows that the first two electrons added to a QD fill the 1s level, and the next six electrons fill the 1p level. We can assume for simplicity that the energy gap between quantum levels is the same, equal to $\Delta = E_Q(3) - E_Q(2) \simeq 20\hbar^2/mD^2$.

We note that formula (3) is valid in the effective mass approximation, when $\Delta \ll E_g$, where E_g is the width of the

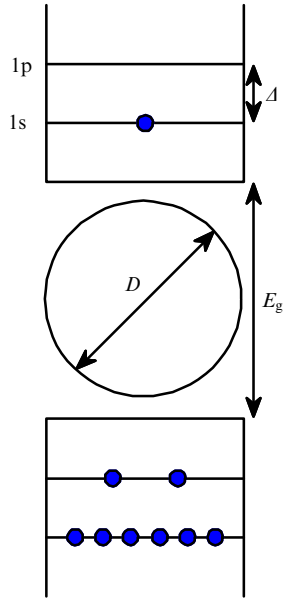

Figure 4. Energy levels in a spherical QD in the simple parabolic model. The conductivity band and the valence band in the bulk semiconductor are separated by the gap E_g. Because the QD diameter D is small, kinetic energy levels in a QD are quantized in accordance with (3). The first quantization level is denoted by 1s, and the next by 1p. The energy gap Δ between all quantum levels slightly varies from level to level.

semiconducting gap. Otherwise, another approximation would have to be used, where levels are spaced equidistantly with the energy gap $\Delta \simeq c\hbar/D$, where $c \simeq 10^8$ cm s^{-1} [13].

At large filling numbers N, E_Q becomes equal to the Fermi energy $E_F = (3\pi^2)^{1/3}\hbar^2 n^{2/3}/2m$, where $n = 6N/\pi D^3$ is the concentration of electrons in the QD. In making the estimates in this case, we use the expression $E_Q \simeq E_F \simeq N^{2/3}\Delta$, which remains a good approximation even at $N = 1$. The electron wavelength λ_F at the Fermi level is then related to the wave vector k_F and the concentration of electrons as $\lambda_F \sim k_F^{-1} \sim n^{-1/3}$.

For $N \gg 1$, the number of electrons in a QD can be measured based on optical absorption. For small N, indeed, optical transitions from the occupied 1s level to the 1p level are possible. The energy of this transition is equal to Δ, but for $N \gg a_B/D$, plasmon absorption at the frequency $\omega_p \sim \sqrt{Ne^2/\kappa_{QD} m D^3}$ can be observed in optics. The transition between two regimes was experimentally observed in [62]; it occurs when $\hbar\omega_p$ becomes comparable to Δ.

3.2 Electrostatic energy

We next consider the energy required to change the charge of a QD.

Calculating this energy is quite complicated if donors in the QD are located randomly. But there is a simple approximation, applicable as long as the QD dielectric constant κ_{QD} is much larger than the average dielectric constant κ of the QD array as a whole, i.e., $\kappa_{QD} \gg \kappa$.

The large value of κ_{QD} implies that any internal charge q is totally compensated by the dielectric response of the QD, which leads to a redistribution of most of the charge $q(\kappa_{QD} - \kappa)/\kappa_{QD} \simeq q$ on the QD surface. In this sense, in calculating the Coulomb interaction, each QD can be regarded as a metal sphere. In particular, the energy of a QD with charge q is equal to $qe^2/\kappa D$, similarly to the constant interaction approximation [63].

Table. Main parameters of a QD array.

QD	a_B, nm	Δ, eV	κ	E_c, meV	Δ/E_c	t, meV
Si	2.0	0.2	3.1	87.7	2.3	1.4
CdSe	4.4	0.5	2.8	97.1	5.1	3.4
PbS	98.2	0.1	68.7	6.3	16	0.7

In this approximation, the energy necessary to add one electron to a neutral QD is

$$E_c = \frac{e^2}{\kappa D}\,. \tag{4}$$

The calculation of κ is described in Section 4.1. As regards the estimate of κ_{QD}, we note that κ_{QD} coincides with the permittivity of the bulk material. An argument in favor of this approach is that, as the size of QDs decreases, their permittivity is practically unchanged. For example, it was shown for a silicon QD in [64] that, as the diameter decreases from four to two nanometers, the dielectric constant changes inconsiderably: it decreases from 10 to 8. The decrease is related in [65] to a dispersion dependence of the dielectric permittivity $\kappa_0(k)$ in the bulk material, with $\kappa_{QD} \sim \kappa_0(1/D)$.

To proceed with the discussion of the conductivity of a QD array, it is helpful to have estimates of the principal characteristics of arrays of QDs made of some materials. In the table, instead of the dielectric constant of the QD material (κ_{QD}) and the effective electron mass, we give geometric means of the corresponding parameters from [66]. For estimates, it is assumed that QDs have a typical size $D = 5$ nm and touch each other with their faces of a typical size $\rho = 1$ nm, the dielectric constant of the medium is $\kappa_i = 1$, a_B is the Bohr radius, and Δ is the energy difference between the 1s and 1p levels (Eqn (3)). The dielectric constant κ for a QD array is calculated by the Maxwell–Garnett formula (9). Here, E_c is charging energy (4) and t is overlap integral (11). In calculating Δ for a QD made of PbS, the nonparabolicity of the band structure was taken into account, and formula (8) was used for dielectric permittivity.

3.3 Model applicability conditions

If electrons appear in a QD due to doping, then the following applicability conditions arise for the model under consideration.

The electrons can be localized on donors. For the applicability of the model, the electron wave functions must be delocalized in the QD, and the expression for kinetic energy (3) is valid when $D < 6a_B$ [67]. This condition follows from the simple observation that the kinetic energy Δ of an electron in a quantum well must be greater than the Coulomb potential holding the electron on the donor, $e^2/\kappa_{QD} a_B$.

Energy levels (3) in a QD are multiply degenerate. However, with strong doping, with the number of electrons

$$N \gg \left(\frac{a_B}{D}\right)^3, \tag{5}$$

the degeneracy of energy levels is lifted. Under this condition, the particles can actually be considered metallic, having a random distribution of energy levels and the typical distance between them being $\delta = \Delta/N^{1/3}$. This case is the subject of

numerous studies (see, e.g., [19, 68]). We comment on the satisfaction of this condition.

Under strong doping, the average numbers of donors and electrons coincide. For large N in (5), the random distribution of donors in a QD must be taken into account, which produces a typical electric field $\mathcal{E} = \sqrt{N}e/\kappa_{\rm QD}D^2$. In this electric field, Stark splitting of levels occurs. We note that the matrix element of the electric field potential is equal to $e\mathcal{E}D$ only for transitions with the orbital quantum number changed by unity; otherwise, it is equal to zero. Because the energy gap between such levels is of the order of $N^{1/3}\Delta$, the typical Stark splitting in the second order of the perturbation theory is given by $(e\mathcal{E}D)^2/N^{1/3}\Delta$. The Stark splitting of levels starts playing a role and becomes comparable to Δ when condition (5) is satisfied.

As noted above, QDs can have a characteristic faceting, with the faces having a typical size ρ. Certainly, the strong level degeneracy, inherent in spherically symmetric QDs, Eqn (3), is then lifted. This is inessential for low-lying levels. The effect is significant for higher levels, when the typical level splitting is comparable to Δ, which is the case for $\lambda_{\rm F} \ll \rho$. As we show in what follows, under this condition an array of QDs that touch each other is in the metallic state, in which the detailed positioning of levels in an individual QD is unimportant. Under the same condition, an array of nontouching QDs cannot be in the metallic state. The estimate for the highest filled level $E_{\rm Q} \simeq E_{\rm F}$ still holds, and therefore the effects discussed here are relevant.

4. Array of quantum dots

4.1 Dielectric constant

In passing from a single QD to a QD array, we must consider a number of new conditions and parameters. We recall that for simplicity we here consider an array in which the QDs are arranged into a simple cubic lattice with the period $D' \simeq D \gg s$ (Fig. 1a).

First of all, it is necessary to take into account that the dielectric permittivity κ of an array can be substantially different from the dielectric permittivity of the material of QDs. In the general case, κ depends on $\kappa_{\rm QD}$, the dielectric permittivity κ_i of the medium around the array, and the volume fraction f of QDs in the array. We note that for the simple cubic lattice of QDs separated by a distance $s > 0$ (see Fig. 1), $f = \pi D/6(D+s)$.

The dependence $\kappa(\kappa_{\rm QD}, \kappa_i, f)$ is sought in a number of papers [69]. Estimates can be obtained assuming different relations between the parameters. In [70], the limiting case is considered that allows an exact solution for any value of f, but for a small difference between the dielectric permittivities: $\kappa_{\rm QD}/\kappa_i \simeq 1$. In this approximation, it is possible to write the expression for κ as

$$\kappa^{1/3} = (1-f)\kappa_i^{1/3} + f\kappa_{\rm QD}^{1/3}\,. \tag{6}$$

At small concentrations $f \ll 1$ and any ratio of the dielectric permittivities,

$$\kappa = \kappa_i + f\frac{3(\kappa_{\rm QD}-\kappa_i)\kappa_i}{\kappa_{\rm QD}+2\kappa_i}\,. \tag{7}$$

In those cases where nanoparticles touch each other, $f \simeq \pi/6$, and the dielectric permittivity is high, $\kappa_{\rm QD}/\kappa_i \gg 1$,

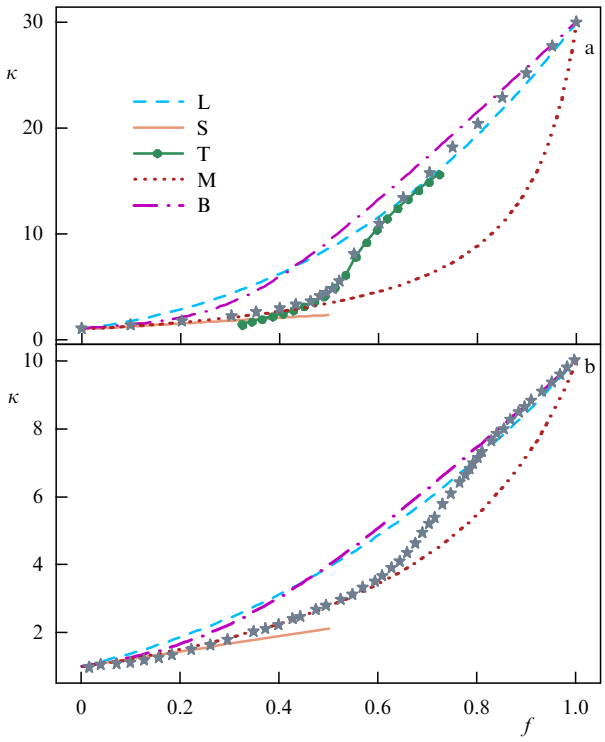

Figure 5. Dependence of the dielectric permittivity κ of a QD array on the dielectric permittivity $\kappa_{\rm QD}$ of the QD and the fraction f of QDs, with the dielectric permittivity of the medium $\kappa_i = 1$. Numerical computations in [72, 73] are represented with stars: (a) $\kappa_{\rm QD} = 30$ and (b) $\kappa_{\rm QD} = 10$. Dependences (6) to (10) are shown with the respective lines L, S, T, M, B.

another relation was obtained in [71], depending on the parameter $s = D' - D$:

$$\kappa(s) = \begin{cases} \dfrac{\pi}{2}\kappa_i\left(\dfrac{D}{2s+2\delta}\right)^{1/3}, & s > 0\,, \\ \kappa_{\rm QD}\sqrt{2\dfrac{|s|+\delta}{D}}\,, & s < 0\,, \end{cases} \tag{8}$$

where $\delta \simeq 0.8D(\kappa_i/\kappa_{\rm QD})^{6/5}$. Here, the domain of negative s corresponds to QDs whose faces touch each other. The typical size of the face is $\rho = \sqrt{|s|D/2}$.

These results are exact under the specified conditions, unlike the frequently used expressions of mean-field theory, the Maxwell–Garnett approximation [69]

$$\kappa = \kappa_i\frac{\kappa_{\rm QD}+2\kappa_i+2f(\kappa_{\rm QD}-\kappa_i)}{\kappa_{\rm QD}+2\kappa_i-f(\kappa_{\rm QD}-\kappa_i)} \tag{9}$$

and the Bruggermann approximation [69]

$$(1-f)\frac{\kappa_i-\kappa}{\kappa_i+2\kappa} + f\frac{\kappa_{\rm QD}-\kappa}{\kappa_{\rm QD}+2\kappa} = 0\,. \tag{10}$$

It is instructive to compare the applicability of the various approaches to assessing κ with known numerical results [72, 73] obtained for a cubic array of spheres with $\kappa_{\rm QD} = 30$, $\kappa_{\rm QD} = 10$, and $\kappa_i = 1$.

These data are presented in Fig. 5 together with dependences (6)–(10). We can see that the dependences describe the numerical results sufficiently well in the range of their applicability.

In the case of a moderate difference between dielectric permittivities, $\kappa_{\rm QD}/\kappa_i = 10$, the Maxwell–Garnett formula works perfectly well, but expression (8) then gives a poor

description, not shown in Fig. 5b. In the case of large dielectric permittivities, only formula (8) gives a satisfactory result when the QDs touch each other ($s = 0$, $f = \pi/6$).

The approaches discussed in this section are, strictly speaking, applicable for calculating dielectric permittivities in a planar capacitor, i.e., at long distances. Just this dielectric constant enters the conductivities of the insulating state of the QD array, when hops occur over long distances. At short distances, the field in the array is strongly inhomogeneous, and this can significantly affect the energy E_c of charging a neutral QD. In [71], manifestations of this effect were considered in the worst-case scenario: for touching QDs and in the case of large dielectric permittivities, $\kappa_{QD} \gg \kappa$. It turned out that the value of E_c is approximately 50% higher than the one following from (4). The exact coefficient depends on the lattice type. For example, for the simple cubic lattice, as shown in [71], this coefficient is equal to 1.6. This is exactly how the value of E_c for PbS, as given in the table, was calculated. For simplicity, without losing the generality, we disregard this coefficient.

4.2 Overlap integral

To describe the transport properties of an array of QDs, the overlap integral t between two QDs must be known.

In a QD array, each energy level (3) is split, with the magnitude of the splitting $\simeq t$. But even if QDs are touching, we typically have $t \ll \Delta$, and in the first approximation we can assume that spectrum (3) changes inconsiderably. In the approximation $t \ll \Delta$, under the condition that the electron is at the lowest, 1s, energy level and the QDs touch one another with their faces of a typical size ρ (Fig. 6), the formula

$$t = \frac{8}{3\pi}\Delta\left(\frac{\rho}{D}\right)^3 \tag{11}$$

was obtained in [74].

Deriving the expression for t requires solving the problem of a wave with $\lambda \sim D$ (where λ is the wavelength) passing through an opening of radius $\rho \ll D$. This problem has been known for a long time: for acoustic waves, it was solved by Rayleigh [75], and for microwaves, by Bethe [76]. In the general case, Levine and Schwinger solved it for a scalar plane wave [77]. We now derive expression (11) up to a numerical coefficient.

We let ψ_0 denote the wave function of an electron in the 1s state in an isolated QD (see Fig. 6). Normalization to the bulk gives the typical wave function $\psi_0^2 D^3 \sim 1$, with the wave function vanishing on the QD surface. We now consider two

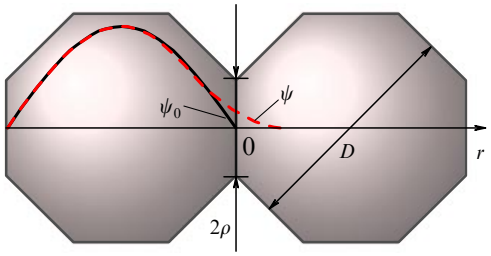

Figure 6. QDs of a typical size D touch one another with their faces of a typical size ρ in the plane $r = 0$. If the QDs do not touch, then the electron wave function on the 1s level, ψ_0, vanishes on the boundary. As the QDs touch, the electron wave function ψ 'leaks' to the neighboring QD, decaying over the distance ρ.

QDs that touch each other with their faces of size ρ in the plane $r = 0$. Because ψ_0 vanishes at the QD boundary, the overlap integral between the wave functions ψ_0 in the "right" and "left" QDs is zero. Hence, to calculate t, we must take into account that the electron wave function ψ in the left QD extends to the neighboring right QD through the area of the contact. Such an approach was used, for example, to calculate the H_2^+ states in [78, 79]. In the plane $r = 0$ and in the right QD, the wave function ψ does not vanish and decays over a typical distance ρ. The derivative $\partial\psi/\partial r \simeq \partial\psi_0/\partial r$ in the plane $r = 0$ then weakly depends on ρ. Therefore, by the order of magnitude, the wave function in the plane can be estimated as

$$\psi(r = 0) \simeq \rho\frac{\partial\psi_0}{\partial r} \simeq \frac{\rho}{D^{5/2}}\,.$$

The matrix element t for the electron is given by Bardeen's formula [80, 81]

$$t = \frac{\hbar^2}{m}\int \psi^*\frac{\partial}{\partial r}\psi\,\mathrm{d}S\,,$$

where integration is over the contact area S in the plane $r = 0$. This actually reflects the fact that the matrix element $t = \hbar/\tau \sim \int j\,\mathrm{d}S$ is related to the time τ of electron oscillations between the QDs and the electron density flux j through the boundary.

Substituting expressions for the wave function and its derivatives in Bardeen's formula, we obtain (11).

The result in (11) was generalized in [82] to three practically important cases: the electrons are not exclusively located on the 1s level; the QDs do not touch each other with their faces but are separated by a distance s; and the masses of the electrons in the QD, m, and in the ambient medium, m^*, are different.

In the first case, we must take into account that the wave vector of an electron on a higher level is $k_F = \lambda_F^{-1} \gg D^{-1}$; t can then be written as

$$t \sim \Delta(k_F\rho)^3\,. \tag{12}$$

In the second case, QDs can be regarded as spheres. Because of a finite distance $s = D' - D$ between the QDs, the wave functions decay exponentially, and so does $t \propto \exp(-s/b)$, where $b = \hbar/\sqrt{2m^*\varphi}$ is the decay length of the electron wave function in the ambient medium, which is determined by the finite work function φ needed for extracting an electron from the QD.

In the general case, the result for t can be represented as

$$t \simeq \Delta\exp\left(-\frac{s}{b}\right)\begin{cases} k_F^3 b^2 D\dfrac{m^*}{m}\,, & \dfrac{m^*}{m} \ll \dfrac{1}{k_F b}\,, \\ k_F D\dfrac{m}{m^*}\,, & \dfrac{m^*}{m} \gg \dfrac{1}{k_F b}\,. \end{cases} \tag{13}$$

We note that for the first energy level, $k_F \sim 1/D$, and under the condition of a large work function $\varphi \gg \Delta$, expression (13) reproduces the result in [83] up to numerical factors.

Qualitatively, the dependence of t on the mass ratio m^*/m and the wave vector k_F is shown in Fig. 7. We can see that t is close to the maximum value only in a narrow range of parameter values.

We emphasize that, for spherical particles in the case $m^*/m \ll (k_F b)^{-1}$, the expression for t can still be written as in (12) with $\rho = \rho_b = \exp(-s/3b)(b^2 D m^*/m)^{1/3}$. Expression

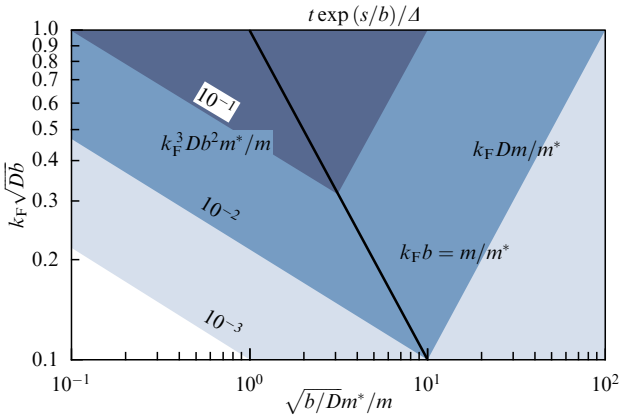

Figure 7. Schematic dependence (13) of the overlap integral t on the electron wave vector k_F in a QD; b is the decay length of the wave function in the ambient medium, m/m^* is the ratio of the effective mass in a QD to the mass in the ambient medium, s is the distance between QDs. Color shows the domains in which t changes by an order of magnitude. The thick line shows the parameter at which transition from one regime to another occurs ($k_Fb = m/m^*$).

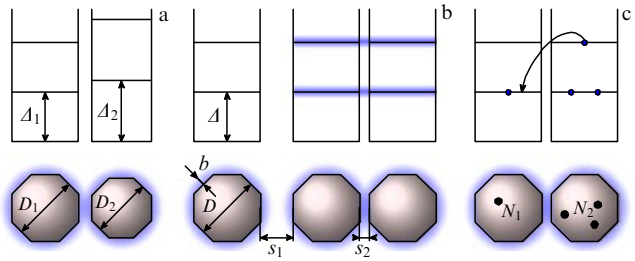

Figure 8. Three possible types of disorder in a QD array. The typical QD size is D, the distance between QDs is s. The electron wave function decays at a distance b, which is illustrated by the blue area around the QD. The kinetic energy of electrons in a QD is quantized in accordance with (3). A typical distance between energy levels is Δ. (a) The first disorder type is associated with variations in the QD diameters; (b) the second with variations in distance; (c) and the third with variations in the number of donors in the QD.

(12) can also be easily generalized to the two-dimensional case: for example, for graphene QDs that touch one another, $t \sim \Delta(k_F\rho)^2$.

In the general case, increasing the overlap integral requires increasing the number of electrons in the QDs, for example, by doping.

All the details of the band structure of the QD material and the QD shape are disregarded in this approach.

In a number of studies [57, 84, 85], the strong-coupling method was used to calculate band diagrams for a lattice of PbSe and CdSe crystals touching one another. We compare the results of calculating t from expression (11) with those obtained in [57] for CdSe QDs.

For this, we map the computation parameters in [57] into the corresponding quantities of the model under consideration. For the energy gap Δ between quantum levels, this gives $\Delta \simeq 0.4$ eV. The QDs in [57] touch with their faces. Assuming that the contact area is $\pi\rho^2$, we find that $\rho/D \simeq 0.25$. In accordance with (11), we obtain the band width for the square lattice $8t \simeq 0.041$ eV, which is only one half the result obtained in [57]. The difference can be attributed to the nonsphericity of particles and to the fact that formula (11) is exact only in the limit $\rho \ll D$.

Knowing the overlap integral between particles, it is easy to calculate the band structure for electrons in a QD array. But this approach does not take an important circumstance into account, the presence of disorder in the system, which is persistent in some cases. We next proceed to this situation.

4.3 Disorder in a QD array

In the absence of disorder and with an arbitrarily small overlap integral, the energy bands of an array are formed from quantum levels of the individual QDs. Disorder is an obstruction to this. In the simplest case of geometric disorder, the QD sizes or the distance between QDs changes (cases a and b in Fig. 8).

We discuss these cases in detail.

We begin with the first case, shown in Fig. 8a. The diameter of a particle can vary from particle to particle, $D = \bar{D} \pm \delta D$; modern technology allows attaining the root-mean-square deviation of QD diameters equal to 5%: $\alpha = \delta D/\bar{D} = 0.05$ [45, 86]. We note that, for particles 5 nm in diameter, this precision corresponds to a size variation of one atomic layer [87]. Such a spread between the diameters must result in the energy spread $E_Q = \bar{E}_Q \pm \gamma_A$ from particle to particle compared with the mean $\bar{E}_Q$, where

$$\gamma_A = 4\alpha\bar{E}_Q \simeq \alpha N^{2/3}\Delta\,. \tag{14}$$

This disorder is similar to the Anderson model disorder.

In the case where the QDs are covered with ligands, the distance $s = \bar{s} \pm \delta s$ between them can vary around the mean $\bar{s}$, for example, due to different ligands densities on the faces or due to temperature fluctuations.

This case of varying distances (Fig. 8b) is close to the Lifshitz model of disorder [88]. As a similarity to that model, we note the following. The overlap of the wave functions of the nearest QDs leads to a shift of quantum levels. These shifts are different for different QDs because each QD is in a different environment. The spread of distances must result in the energy spread $E_Q = \bar{E}_Q \pm \gamma_L$ from particle to particle, where

$$\gamma_L \sim t(\bar{s})\,. \tag{15}$$

In the cases listed above, we addressed the one-electron problem. Such an approach is applicable when electrons are induced in a field transistor based on a QD array (see Sections 6.3–6.5 below).

Under doping, another type of disorder can appear, as shown in Fig. 8c, one associated with the impossibility of ensuring equal numbers of impurity donors in each QD. We now discuss this case.

The probability that a QD has exactly N_d donors is given by the Poisson distribution

$$P(N_d) = \frac{N^{N_d}}{N_d!}\exp(-N)\,. \tag{16}$$

The variation in the number of donors from one QD to another is $N_d = N \pm \sqrt{N}$; we recall that the average number of donors is equal to the average number N of electrons in QDs (and we let N denote both these numbers in what follows). The variation in N_d leads to a variation in the Fermi level in individual QDs: $\delta E_F \simeq E_F/\sqrt{N} \simeq N^{1/6}\Delta$.

In an array, the QDs must share a common Fermi level, and therefore the electrons are redistributed between the

QDs, which in turn leads to the number of electrons not matching the number of donors in some QDs, making such QDs charged (Fig. 8c). As a result, the array consists of randomly charged QDs in a random Coulomb field.

We estimate the typical QD charge Q when the Fermi level is equalized [82]. The redistribution of electrons stops when the initial fluctuations of the Fermi level in individual QDs δE_F are compensated by the Coulomb potential of each QD: $QE_c \simeq \delta E_F$, whence $Q \simeq N^{1/6}\Delta/E_c$. This expression for Q is valid in the case where $N^{-1/6} \ll \Delta/E_c \ll N^{1/3}$, the two inequalities corresponding to two constraints on Q. First, Q cannot be less than unity. Second, Q cannot be greater than the initial fluctuation of electrons in QDs, $\sqrt{N}$, which corresponds to the fluctuation of donors (see above). At a high ratio $\Delta/E_c \gg N^{1/3}$, the Coulomb effects are unimportant, and the electrons redistribute freely, i.e., $Q \sim \sqrt{N}$. Finally, for $\Delta/E_c \ll N^{-1/6}$, the Coulomb effects are so strong that no charging occurs: $Q = 0$.

We make the estimates under the assumption that $\kappa_{QD} \simeq \kappa$, because no detailed analysis of charge redistribution has been done in the literature with the difference between two dielectric constants taken into account. In this approximation, the condition $\Delta/E_c \ll N^{1/3}$ is similar to condition (5), under which QDs can be considered metallic.

We estimate the fluctuation of the random Coulomb potential in the case of interest where $\Delta/E_c \gg N^{1/3}$. The QD array can then be regarded as a strongly doped semiconductor with the electron concentration $n \simeq N/D^3$, the density of states $g \sim n/E_F \sim N^{1/3}/\Delta D$ at the Fermi level, and the screening radius

$$r_0 = \sqrt{\frac{\kappa}{4\pi e^2 g}}, \tag{17}$$

whence $r_0 \sim D\sqrt{\Delta/N^{1/3}E_c} \gg D$.

Fluctuations of the potential $e^2\sqrt{nr_0^3}/\kappa r_0$ lead to a shift of energy levels in some QDs compared with others by the quantity

$$gamma_S = N^{5/12}E_c\left(\frac{\Delta}{E_c}\right)^{1/4}. \tag{18}$$

From the experimental standpoint, it is interesting to discuss whether the effect of the redistribution of electrons can be revealed by the quantum photoluminescence yield of a QD array.

It is known that the existence of an additional electron in a QD leads to the nonradiative Auger recombination of a photoexcited electron–hole pair. In this process, the annihilation energy of the pair is transferred to the additional electron. Because the rate of nonradiative Auger processes is much higher than the rate of radiative recombination [89], even a single extra electron can suppress the photoluminescence of QDs with a probability of almost 100%. In other words, only "empty" QDs, i.e., those without an electron, make a contribution to photoluminescence. This problem was investigated theoretically for an array of doped QDs in [90], where it was shown that at the average number of donors greater than two, $N > 2$, the QD array produces no photoluminescence. A similar problem of the suppression of photoluminescence by additional electrons induced in a field transistor was investigated experimentally in [91].

Among the important types of disorder in QD arrays are those due to the presence of impurities in the ambient medium. For example, a QD can be doped via ligands

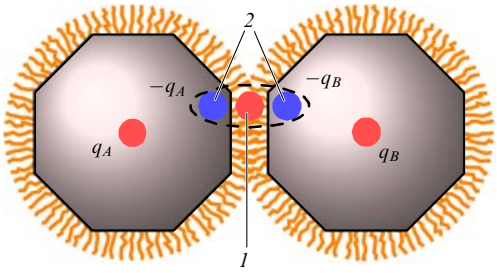

Figure 9. (Color online.) Fractionalized charge of a surface donor in a QD array. The positive charge $+e$ of the donor (shown in red, *1*) due to image forces induces negative charges $q_{A,B}$ in the neighboring QDs (shown in blue, *2*), which completely neutralize the positive charge of the donor, $q_A + q_B = +e$, because $\kappa \ll \kappa_{QD}$. Positive charges $q_{A,B}$ then form at the center of the corresponding QDs.

located on the surface [47, 48]. This type of disorder plays a decisive role in electron transport in metallic nanoparticles [19, 92]. We make a brief detour to consider it in somewhat greater detail (Fig. 9) [92, 93]. The argument adduced here, strictly speaking, is valid for metallic nanoparticles, but in the case where the dielectric permittivity κ of the array is much less than the dielectric permittivity κ_{QD} of the QD material, the QDs can be regarded as metallic in the first approximation.

We consider a donor near the surface of two QDs in a medium with $\kappa \ll \kappa_{QD}$. The positive charge $+e$ of the donor creates a negative image charge $-q_{A,B}$ in neighboring QDs, such that $q_A + q_B = +e$. Because the QDs must be neutral overall, an equal but positive charge $q_{A,B}$ appears in the center of each QD. The potential of the donor and two of its images are short range, and can therefore be disregarded. The distribution of electrons is affected only by the potential created by the charges in the center. Hence, the original positive charge of the donor is fractionalized (split) into noninteger charges $q_{A,B}$. Obviously, when there are numerous donors around the QD, their fractionalized charges are added up. Finally, we must recall that each donor brings an electron into the array. These electrons are redistributed in the QD array so that their total energy is minimal. We see that this disorder is largely analogous to the are occurring in doping a QD array.

We have considered the main disorder types, but others are not excluded. For example, a lattice of touching QDs made of PbSe can exhibit disorder related to changing the sign of the overlap integral t [94] from one QD to another. This can also lead to localization of electrons.

It is worth noting that different types of disorder can be related to each other. For example, disorder in QD sizes inevitably leads to disorder in the distances between QDs [87].

4.4 Density of states

In a QD, the distribution of the density of states over energies is given by peaks with the period Δ (Fig. 10). Geometric disorder leads to the widening of the peaks; the peak width is then equal to the larger of two values γ_A and γ_L (Fig. 10a).

Under doping, the density of states $g(\varepsilon)$ of an array is quite different from the density of states in individual QDs. We proceed to considering $g(\varepsilon)$ near the Fermi level ε_F in this case.

We first consider the case where disorder is absent in the system, i.e., the numbers of electrons and donors are the same in all QDs.

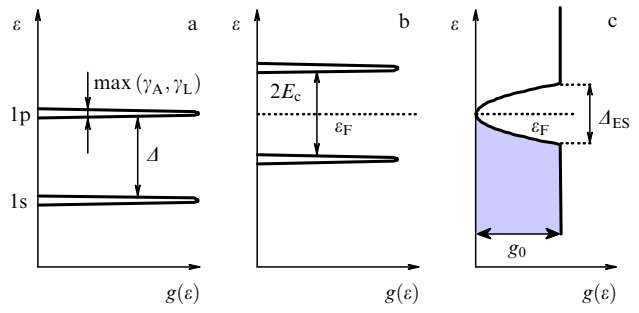

Figure 10. Density of states $g(\varepsilon)$ in a system of QDs. In an individual QD, energy levels are distributed practically periodically with the period Δ. (a) Without the Coulomb effects, each peak widens due to geometric disorder. (b) With the Coulomb interaction taken into account, two peaks with the energies ε_F appear near the Fermi level $\pm E_c$. (c) Under strong disorder, the density of states is washed out, but a Coulomb gap of the width Δ_{ES} appears at the Fermi level.

We discuss this case for a QD containing only five donors [93] and assume that the Fermi level coincides with the 1p level of an individual QD, i.e., $\varepsilon_F = E_Q(n = 5)$ (Fig. 10b). As the electron moves from one QD into another over an infinitely long distance, these QDs acquire opposite charges, and the energy of each charged QD is equal to E_c. Hence, the density of states is symmetric with respect to the Fermi level and consists of two δ-peaks with $\varepsilon = \varepsilon_F \pm E_c$.

We now consider a more realistic case where the numbers of electrons and donors in an individual QD are different. We want to see how this disorder affects the density of states [93]. Obviously, for a small number of donors, $N \ll 1$, the situations does not change dramatically compared with the case without disorder. Indeed, under the condition $N \ll 1$, there are practically no QDs with more than three donors: according to distribution (16), the number of QDs is $N^3/6 \ll 1$. This means that there are practically no electrons that can occupy the 1p electron shell, and hence there is no redistribution of electrons over the QDs. In this case, similarly to the preceding one, the density of states is also given by two δ-peaks with $\varepsilon = \varepsilon_F \pm E_c$, where the Fermi level coincides with the 1s level.

Although we have restricted ourselves to the case $\Delta \gg N^{1/3}E_c$, we can also infer some conclusions as to what is to happen in the case of the inverse relation, when the QDs are metallic. In that case, no recharging of the system occurs either, all QDs are neutral, and moving an electron requires recharging two QDs, whence $g(\varepsilon) = \delta(\varepsilon_F \pm E_c)$.

In [93], the general case $N \gg 1$ was considered numerically. The results in [93] agree with those obtained later in a more general form [82]. In what follows, we restrict ourselves to only considering the results of this last paper.

Two types of disorder were considered in [82]: in size and in the number of donors for a system of QDs touching one another with their faces of a typical size ρ. We recall that QDs whose faces do not touch can also be considered to have an effective touching radius $\rho = \rho_b$ (see Section 4.2). The obtained results are illustrated in Fig. 11. We explain the main conclusions.

We begin with the case $\alpha(D/\rho)^2 \gg 1$, which is shown in Fig. 11a. Four parameter domains can be selected: I (insulator), OI (oscillating insulator), M (metal), and I′ (insulator with metallic QDs). Each domain was identified based on the form of the density of states.

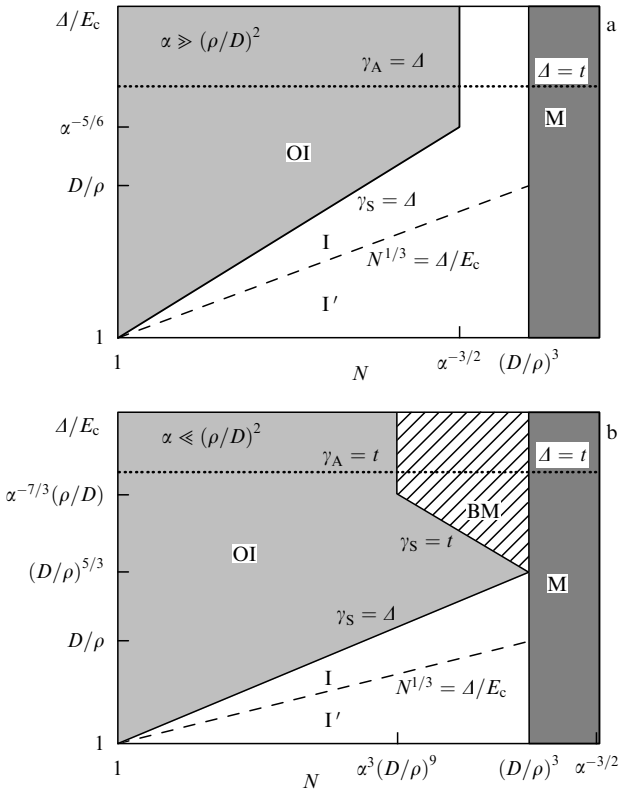

Figure 11. Possible states of an array of QDs of size D, touching over the faces of size ρ, as a function of the parameters Δ/E_c and N for (a) high and (b) low disorder α in size. Notation used in the figure: I — insulator, OI — oscillating insulator, M — metal, I′ — insulator with metallic QDs, BM — blinking metal. The upper dashed line shows the values at which the localization length ξ in Fig. 12 is evaluated. Next to each line separating the states, its defining equation is given.

In the domain designated by OI in the phase diagram, we have $\gamma_S, \gamma_A \ll \Delta$, disorder is sufficiently low, and hence the density of states is given by peaks with the period Δ and with the width equal to the larger of the two values γ_S and γ_A.

In domain I, disorder of one of the types is so strong that the density of states is practically uniform. For example, if $\gamma_A \gg \Delta$, i.e., $N > \alpha^{-3/2}$, then variation of the energy E_Q from QD to QD is greater than Δ. The levels E_Q in each QD are positioned practically periodically, and, therefore, irrespective of the level shift from one QD to another, the difference between the QD energies cannot exceed Δ; as a result, the density of states is uniform over the QD array.

Domain I′ is similar to domain I, but the QDs exhibit metallic properties (see Eqn (5)).

In domains OI and I, the QD array is in the insulating state, but in OI the conductivity properties strongly depend on the position of the Fermi level. This case is considered in detail in Section 4.5.

In domain M, with $N \gg (D/\rho)^3$, when $\Delta \ll t$ (see Eqns (1) and (11)), the system is in the metallic state (see Section 5 below). The density of states is practically uniform over the entire energy spectrum.

Figure 11b illustrates another case: $\alpha(D/\rho)^2 \ll 1$.

As in the preceding case, there are four domains of the parameters, I and OI, M, and I′, but an additional domain BM, whose boundaries are defined by the conditions $\gamma_S = t$, $\gamma_A = t$, and $\Delta = t$, also appears. In this domain, the density of states exhibits periodic peaks with the width equal to the

larger of the two values γ_S and γ_A and with the period Δ. The difference between this and the OI phase is that, when the Fermi level is positioned in the middle of such a peak (in accordance with $t > \gamma_S, \gamma_A$), the electrons are delocalized. For this reason, this domain was called a blinking metal, because metallic properties manifest themselves only for a certain position of the Fermi level. We note that a similar behavior is also observed in the well-known quantum Hall effect [95].

Two approximations for the density of states of a QD array were used in the foregoing: the density of states vanishes between the bands corresponding to the 1s and 1p QD levels; correlations between the electron positions are disregarded. In reality, even in the OI domain, where the density of states changes periodically, the density of states at the mid-point between the bands is small but nonzero.

All the arguments adduced above and the calculations of the density of states pertained to the one-electron approximation. Numerical computations in [93] show that in a QD array, as in bulk semiconductors, taking the electron–electron interaction into account changes the one-particle density of states near the Fermi level. Namely, near the Fermi level ε_F, the density of states $g(\varepsilon)$ must tend to zero faster than ε^2 [96] if the reference value is chosen as $\varepsilon_F = 0$ (Fig. 10c). We clarify this statement by considering an electron system in equilibrium, when the energy of all electrons is less than or equal to ε_F. We move an electron with an energy $\varepsilon_1 < \varepsilon_F$ over a distance r from one QD into another. The new electron state has a greater energy, $\varepsilon_2 > \varepsilon_F$. The electron transfer creates a hole, to which the electron is attracted, which decreases the electron energy by $e^2/\kappa r$. Therefore, for the equilibrium condition to be satisfied in the system, we must have $\varepsilon_2 - \varepsilon_1 - e^2/\kappa r > 0$. This implies that all the electron states in the bulk r^3 are separated from each other by at least the energy $\varepsilon \sim e^2/\kappa r$. Then the density of states is

$$g(\varepsilon) \sim \frac{1}{\varepsilon r^3} \sim \frac{\kappa^3 \varepsilon^2}{e^6} . \tag{19}$$

It hence follows that, as a result of electron–electron correlations, a constant density of states g_0 in the system leads to the formation of a Coulomb gap at the Fermi level of the width $\Delta_{ES} = (g_0 e^6/\kappa^3)^{1/2}$.

4.5 Localization length

An important characteristic of a QD array is the localization length ξ, which shows the typical distance at which an electron is localized. For example, in a weakly doped bulk semiconductor, electrons are localized near donors, and hence $\xi \simeq a_B$. In a QD array, this equality is not satisfied, and we discuss the behavior of ξ in this section.

Up to now, we have been dealing with the electron wave function in an individual QD. In a QD array, the electron wave function decays at long distances $r \gg D$ from QDs as $\Psi \sim \exp(-r/\xi)$. We here note that, as we show in what follows, ξ does affect, although it does not determine, the length of electron hops that make up the hopping conductivity. The hop length, by its meaning, cannot be less than D, but ξ can be less than D. Moreover, it might appear that ξ must be of the order of the decay length of the electron wave function in the ambient medium, outside the QDs $\xi \simeq b \ll D$. But in fact, even if the QDs do not touch each other with their faces, $\xi \gg b$ whenever $D' \simeq D \gg s$. Actually, in tunneling over a distance s from one QD into another, the electron moves over the distance $D' \simeq D$. The probability density amplitude then decreases by $t/\delta E$ times, where δE is the difference between the neighboring QD energies. In tunneling over a distance $r \gg D$, the electron tunnels through $M = r/D$ QDs and its wave function decreases by $(t/\delta E)^M$ times. Rewriting this as $(t/\delta E)^M = \exp(-r/\xi)$, we obtain

$$\xi = \frac{D}{\ln(\delta E/t)} . \tag{20}$$

Even for an exponentially small overlap integral, $t \sim \exp(-s/b)$, we then have [93]

$$\xi \simeq \frac{D}{s} b \gg b . \tag{21}$$

It hence follows that, in the case under consideration, when the QD size is greater than the distance between QDs, $D \gg s$ and ξ is greater than the decay length b of the wave function in the ambient medium $\xi \gg b$.

We see from (20) that the localization length depends on the parameters of the system; it is determined by both disorder in the system, which sets δE, and the overlap integral t.

The localization length has been analyzed in detail where an array of touching QDs features only two types of disorder: by size and by the number of impurities [82]. We now consider this case in detail for large values of Δ/E_c, which are shown with a dashed line in Fig. 11. We analyze the result for high and low disorder in size (Fig. 12).

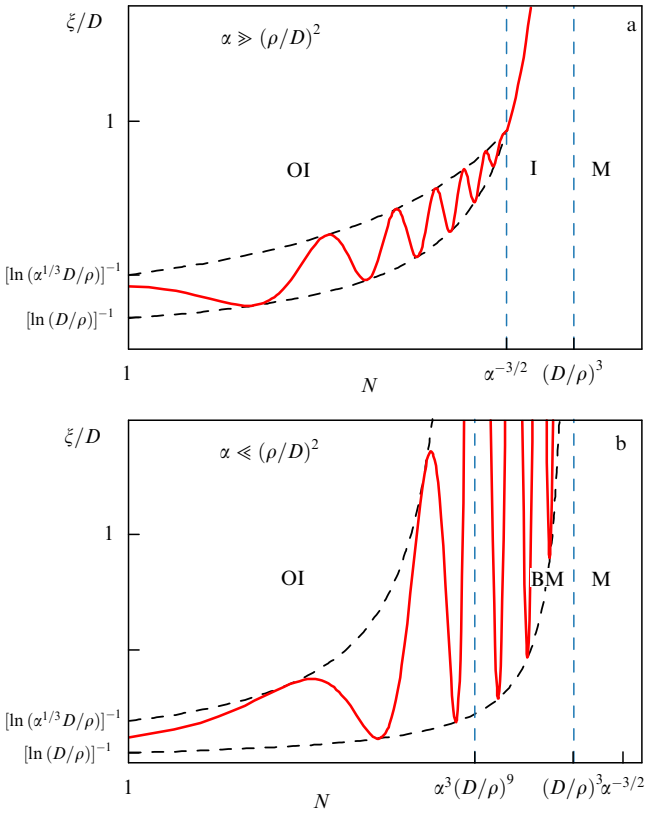

Figure 12. Typical dependence of the localization length ξ on the number of electrons N for QDs of size D that touch each other over faces of size ρ for (a) high and (b) low disorder α in size. The chosen parameter Δ/E_c is shown by a dashed line in Fig. 11; the state of the QD array changes from OI to M. The expressions for maximum (22) and minimum (23) values of ξ are shown by the dashed line. It can be seen that ξ oscillates between maximum and minimum values. In approaching the M and BM states, the maximum value of ξ diverges.

In the case of high disorder, $\alpha \gg (\rho/D)^2$, when the Fermi level is close to the quantum levels of an isolated QD, $\delta E \sim \gamma_A \ll \Delta$, the localization length attains a maximum:

$$\xi \simeq \frac{D}{\ln\left(\alpha D^3/N^{1/3}\rho^3\right)} . \tag{22}$$

When the Fermi level is in the middle of the gap between quantum levels, $\delta E \sim \Delta$, the localization length reaches a minimum:

$$\xi \simeq \frac{D}{\ln\left(1/n\rho^3\right)} . \tag{23}$$

Therefore, the localization length oscillates between the minimum and the maximum with the period $N^{1/3}$, as shown in Fig. 12a. This is why this phase is called an oscillating insulator, OI. As we show below, the conductivity of a QD array must also oscillate as N increases. This behavior of the conductivity was observed, for example, in a CdSe QD array [40].

In the case $\alpha \ll (\rho/D)^2$, as note above, situations are possible where the Fermi level is located inside the delocalized state, $t > \gamma_A, \gamma_S$. The localization length then diverges and the QD array becomes metallic. When the Fermi level leaves one such state, the localization length becomes finite. This occurs when a QD array is in the BM state. Finally, when $t > \Delta$ (i.e., condition (1) is satisfied), the system becomes metallic and the localization length diverges (Fig. 12b).

We have discussed the tunneling of an electron from one QD to another; the QD then remains in the same quantum state. This case is similar to the process of elastic cotunneling in metallic nanoparticles [97], for which inelastic cotunneling has also been considered [68, 98, 99].

Under inelastic cotunneling, the electron leaves an excited electron–hole pair behind. To date, this case has not been discussed for QDs. From the analysis of metallic particles, we can conclude that the effect of inelastic cotunneling starts playing a role at high temperatures, and the quantity ξ must then be temperature dependent.

In principle, expression (20) is invalid near the insulator–metal transition. It was derived based on the tunneling from one QD to another via a particular sequence of QDs and does not take into account that such paths multiply near the transition. However, as we show below, experimental data suggest that, near the transition, $\xi \sim (n\rho_c^3 - n\rho^3)^{-1}$, and hence ξ has the same asymptotic behavior as in expression (23).

5. Metal–insulator transition

Although QDs are semiconductors in and of themselves, an array of QDs can be a metal under certain conditions, and the insulator–metal transition then occurs. This means that electron states are not localized in one QD but are delocalized over the entire array. The problem of the insulator–metal transition in a system of QDs is fundamental [34, 83, 100]. In the case where the QD array features only geometric disorder, this problem corresponds to the one discussed for Anderson and Lifshitz transitions [96]. When the QDs are doped, a new transition criterion emerges, different from the Mott condition for the insulator–metal transition in doped semiconductors. In what follows, we consider the conditions for various types of metal–insulator transitions in an array of QDs: for geometric disorder and doping.

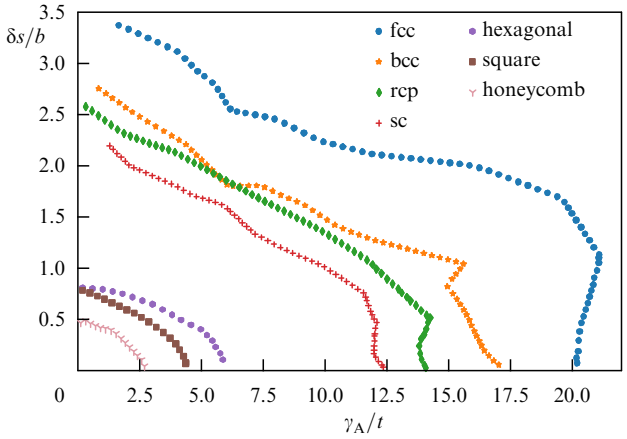

Figure 13. Boundaries of the domain of the γ_A/t and $\delta s/b$ parameters where delocalized states exist in a QD array for various lattice types. The data are from [101]. For small γ_A/t and $\delta s/b$, i.e., on the left of the boundary, delocalized states exist in a QD array. On the right of the boundary, all electron states in the array are localized. Results are presented for three-dimensional lattices: rcp — randomly close-packed, fcc — face-centered, bcc — body-centered, sc — simple cubic; and for two-dimensional lattices: hexagonal, honeycomb, and square. The results obtained in [101] for the coefficient γ_A/t at $\delta s = 0$ correspond to the data known from [96].

5.1 Geometric disorder in a QD array

In the presence of only variations in the size D, as we have noted, the energy of electrons in QDs changes from one QD to another by the quantity γ_A. Anderson delocalization occurs if $t \gg \gamma_A$, the numerical coefficient in this relation being determined by the lattice type (Fig. 13).

In the case of only variations in the distance s, the overlap of wave functions of the nearest-neighbor QDs leads to a shift of quantum levels. These shifts differ for different QDs, because each QD is in a particular environment. Quantum states are distributed in the same way between all QDs only in the case where all the distances between QDs are the same to within the decay length b of the electron wave function. In other words, delocalization of electrons (the Lifshitz transition) must occur when the root-mean-square fluctuation distance between QDs is much less than b: $\delta s \ll b$. Because b can amount to a few angstroms, this is a rather stringent condition. The numerical coefficient involved in this criterion depends on the lattice type (see Fig. 13).

In [101], two geometric disorders were considered jointly and exact values of the coefficients $\delta s/b$ and γ_A/t were calculated at which the transition from the delocalized to the localized state occurs. The result of these calculations for various lattices are also presented in Fig. 13.

We can see from Fig. 13 that the existence of delocalized states of electrons depends on the number of nearest neighbors of a QD in the array: the greater the number of neighbors, the larger the domain of parameters $(\delta s/b, \gamma_A/t)$ where delocalized states can be realized. For example, in a face-centered cubic (fcc) lattice, the number of neighbors is twelve, whereas in a honeycomb lattice, only three, and the respective domains of the parameters supporting delocalization differ seven-fold.

In theoretical paper [83], the overlap integral between QDs covered with ligands was considered in more detail, and it was claimed that QD arrays are possible with delocalized electrons existing in them, i.e., with $t \gg \gamma_A$. This claim is

partially supported experimentally by the observed mobility depending weakly on the temperature, i.e., showing no exponential decrease to zero [59, 102]. But the question of whether this fact is an explicit proof of the transition of the array into the metallic phase remains open. For example, it was stated in [103] that, as the temperature decreases, the distance s between QDs covered with ligands decreases. The array conductivity G depends on this distance exponentially and can therefore increase as the temperature decreases. A clear indication of the insulator–metal transition or the approach to it would be given by the array conductivity obeying the scaling hypothesis, as was shown via the example of a doped QD array. We now proceed to discussing this question.

5.2 Doped QD array

It is well known that, in doping a bulk semiconductor, the metal–insulator transition occurs at donor concentrations n_{M} determined by the Mott criterion $n_{\mathrm{M}} a_{\mathrm{B}}^3 = 0.02$ [104], i.e., when the average distance between donors $n_{\mathrm{M}}^{-1/3}$ becomes comparable to the localization length of an electron on a donor, $\xi \approx a_{\mathrm{B}}$. This dependence works well for many materials and donors as a_{B} ranges three orders of magnitude [35]. It is clear that this criterion must be inapplicable in a system of QDs because of small values of the overlap integral t. If QDs touch each other, then transition criterion (1) can be obtained.

Qualitatively, criterion (1) can be explained as follows. At high concentrations of donors, not only individual QDs but also the entire array has metallic properties. Therefore, the conductivity between two metallic QDs can be calculated by the Sharvin formula [105]

$$G \sim \frac{e^2}{\hbar} (k_{\mathrm{F}} \rho)^2 . \tag{24}$$

Because the transition from the metallic phase to the insulating phase occurs when the conductivity becomes comparable to the minimal metallic conductivity, i.e., $G = e^2/\hbar$ [19, 106], we have $k_{\mathrm{F}} \rho \simeq 1$ at the transition point. Thus, the transition occurs when the typical electron wavelength $\lambda_{\mathrm{F}} \simeq k_{\mathrm{F}}^{-1}$ is comparable to the typical size of the contact between QDs. This last assertion can be rewritten as (1) if we take the relation between the electron concentration n and k_{F} into account.

We note that we can obtain the same criterion (1) by considering the case where the overlap integral t given by formula (11) becomes equal to the distance between quantum levels Δ. From an analysis of expression (24), it also directly follows that, in the metallic phase, the conductivity of the sample must depend on the concentration as $G \sim n^{2/3}$.

Sharvin formula (24) can be given two explanations as follows. The first is based on the Landauer formula [107]: due to the contact between two metallic QDs of area $S \sim \rho^2$, $(k_{\mathrm{F}} \rho)^2$ conductivity channels occur, each of which makes the contribution $e^2/\hbar$. The second explanation is classical: as a bias V is applied between two QDs, electrons acquire a drift velocity v in the direction toward the contact $v/v_{\mathrm{F}} = eV/\epsilon_{\mathrm{F}}$, where v_{F} and ϵ_{F} are the Fermi velocity and energy in the QD. Knowing the current $envS$ running through the contact, it is easy to obtain expression (24) for the conductivity of the contact.

As ρ increases, criterion (1) must pass into the Mott criterion. As show in [82], this happens at $\rho \simeq D$.

Near the metal–insulator transition, the localization length ξ must be much greater than the distance between QDs, $\xi \gg D'$. Consequently, the physics of the metal–insulator transition must be qualitatively the same as in the bulk material, and must follow the scaling hypothesis [108]. In our case, this means that, as the parameter $n\rho^3$ approaches critical value (1), the localization length must diverge as $\xi \sim (n\rho_{\mathrm{c}}^3 - n\rho^3)^{-\nu}$, where ν is the critical exponent. Specific conductivity at the transition point must then have the form $\sigma_{\mathrm{c}} = e^2/\hbar L_\varphi$, where L_φ is the size of the phase coherence domain, which is determined by electron–phonon or electron–electron scattering processes: $L_\varphi \sim T^{-1/z}$ (z is another critical exponent). This substitution gives the specific conductivity value at the transition point $\sigma_{\mathrm{c}} \sim T^{1/z}$, and, near the transition, the specific conductivity must follow the universal law

$$\sigma = \sigma_{\mathrm{c}} F\left(\frac{n\rho_{\mathrm{c}}^3 - n\rho^3}{T^{1/z\nu}} \right), \tag{25}$$

where the function F has two branches corresponding to the insulating and metallic states.

Experimental data in [21, 36, 109] on the conductivity of arrays of ZnO and Si QDs near the metal–insulator transition suggest that the metallic state is not attained in any of the experiments. In [36], the vicinity of the transition in the insulating phase could be reached (Fig. 14) as a result of

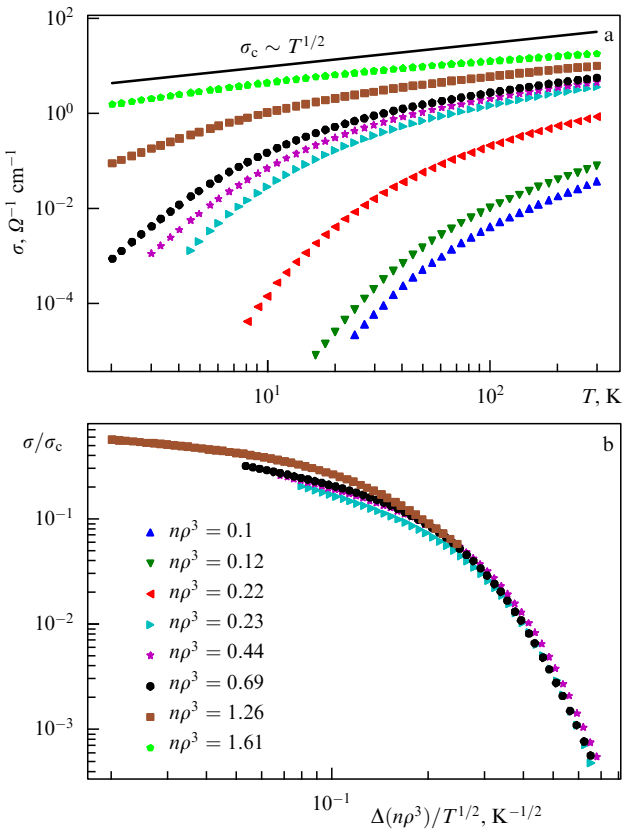

Figure 14. (a) Dependence of the specific conductivity σ of an array of touching ZnO QDs on the temperature T at different sizes of the touching faces ρ and electron concentrations n. The data are taken from [36]. The line $\sigma_{\mathrm{c}} \sim T^{1/2}$ shows the dependence of the conductivity at the transition point. We see that, at $n\rho^3 = 1.6$, the array conductivity is close to the theoretically predicted one. (b) For sample with large σ, the specific conductivity is rearranged in accordance with the scaling hypothesis, Eqn (25). It was assumed that σ_{c} determines the sample with the highest conductivity ($n\rho_{\mathrm{c}}^3 = 1.61$).

increasing both n and ρ (only one branch of dependence (25) was observed). From an approximation of the data, it was derived that $z \simeq 2$ and $\nu \simeq 1.6$. We note that the metal–insulator transition in bulk silicon is characterized by $z \simeq 2$ and $\nu \simeq 1$ [110]. The quantity $z = 2$ is characteristic of electron systems with Coulomb interaction taken into account [111].

In experiment, the insulator–metal transition is not observed at a concentration several times greater than the one given by the estimate in (1). This can possibly be related to the fact that, in deriving (1), the geometry of a QD array was assumed ideal. Deviations from the ideal geometry, for example, rotation of QDs with respect to each other, would lead to an additional scattering of an electron in contacts between QDs, a decrease in t, and an increase in the critical concentration.

We note that the first communication on attaining the transition to the metal phase in a QD array appeared very recently [112].

6. Insulating phase

6.1 Temperature dependence of conductivity

The analysis presented above shows why all the experimental data typically pertain to QD arrays in the insulating phase. As the temperature T decreases in that phase, the electron conductivity G tends to zero exponentially, i.e., in accordance with law (2), where the coefficients p and E_0 are determined by the transport mechanism. Most frequently, experimental conductivity has an activation character, $p = 1$, or follows the ES law, $p = 1/2$, but in some cases a dependence obeying the Mott law $p = 1/4$ is observed. Thus, all types of the temperature dependence of conductivity for QD arrays in the insulating phase are also shared by doped bulk semiconductors, where they are explained in the standard way.

The explanation of these dependences is based on considering a QD array in the form of a network of effective resistances. In this network, the resistance between any two QDs i and j can be defined as the time-averaged rate of electron transitions between QDs i and j divided by the electric field strength in the limit of small fields. Just that is done for the canonical Miller–Abrahams resistance network [96, 113].

From the above considerations, the expression for the resistance between the ith and jth QDs can be written as

$$R_{ij} = R_0 \exp\left(\frac{2r_{ij}}{\xi} + \frac{\varepsilon_{ij}}{kT}\right), \tag{26}$$

where R_0 is a preexponential factor, weakly dependent on the temperature. The first term in the exponent defines how the tunneling probability is suppressed with distance r, with ξ being the localization length described in Section 4.5.

Because the electron is in different energy states in the ith and jth QDs, its transition from the ith to the jth QD requires the energy ε_{ij}, which can be acquired by absorbing a phonon. The second term in (26) shows the probability of that process.

After calculating all the resistances R_{ij} between all QDs, we can find the resistance of the entire array using the percolation approach [96].

We recall the basics of percolation theory. We choose a resistance value R_c, preserve all the resistances in the network for which $R_{ij} < R_c$, and break apart all links between QDs for which $R_{ij} > R_c$ (i.e., set $R_{ij} = \infty$). At some instant as R_c increases from the zero value, an infinite cluster — a critical subnetwork connecting all QDs — is formed. The resistance of the entire system is then equal to R_c, the resistance of this critical subnetwork. A further increase in R_c cannot change the overall resistance of the network significantly, despite its increasing density. New chains, although numerous, leave the resistance virtually unchanged, because they are shunted by the critical subnetwork with a much lower resistance (in accordance with expression (26)). Hence, it is the critical subnetwork that determines the conductivity of a random network of resistances. We must note that, for a QD array, this critical subnetwork, as well as its changes with varying temperature, was observed experimentally in [114]. In Section 6.4 below, we show how the percolation approach can be used to derive less known dependences.

We explain the appearance of a type (2) dependence in a simpler way using Mott's argument.

Temperature dependence (2) is essentially governed by the density of states near the Fermi level of the system. If the density of states has a well-defined size of the gap, for example, consists of periodic delta functions (Fig. 10b), then the dependence of the conductivity on temperature has an activation character. In that case, the conductivity is determined by formula (2) with $p = 1$ and E_0 equal to the gap between the Fermi level and the first unfilled level. For QDs, typical E_0 are by the order of magnitude equal to E_c or Δ. The hops then occur between neighboring QDs, because hops to distant neighbors are not favored by a lower energy required for hopping, as in the cases discussed in what follows.

We consider the case of a constant density of states $g(\varepsilon) = g_0$ near the Fermi level. On neighboring QDs, the energy ε_{ij} is quite large compared with the temperature T, and therefore the probability of hopping to them is extremely low: $\exp(-\varepsilon_{ij}/kT)$. At the same time, on more distant QDs, the energy ε_{ij} can be small, but the tunneling probability is also small: $\exp(-r_{ij}/\xi)$. Thus, there is competition between two processes. A "long-distance hop" has low probability, but the longer the hop, the higher the probability of an electron finding a QD with small ε_{ij}.

We clarify why $p = 1/4$ in this case. We consider electrons with energies $\varepsilon_{ij} = \varepsilon_M$ in a narrow strip near the Fermi level. All these electrons are in QDs whose concentration is $\mathcal{N}(\varepsilon_M) = g_0\varepsilon_M$, the average distance between such QDs being $r_{ij} = \mathcal{N}^{-1/3}(\varepsilon_M)$. From (26), we obtain the resistance that can ensure hops over the QDs belonging to the energy strip:

$$R = R_0 \exp\left(\frac{2}{\mathcal{N}^{1/3}(\varepsilon_M)\xi} + \frac{\varepsilon_M}{kT}\right). \tag{27}$$

Due to the competition between two processes, the resistance has a narrow minimum at $\varepsilon_M \sim (kT)^{3/4}/(g_0\xi^3)^{1/4}$. Transport is effected only by electrons from this narrow energy strip ε_M, and the resistance is given by formula (2) with $p = 1/4$ and $E_0 = \varepsilon_M \sim (g_0\xi^3)^{-1}$. The coefficient in the last relation is determined by percolation theory; for a bulk semiconductor, it is equal to 28.3 [96] and must be the same for a QD array. By the order of magnitude, the length of a typical hop is $r_M \sim \mathcal{N}^{-1/3}(\varepsilon_M) \sim \xi(\varepsilon_M/kT)^{1/4}$.

Near the Fermi level, as we saw in Section 4.4, the electron–electron correlations result in a Coulomb gap. Using the density of states near the Fermi level in form (19) and invoking the same argument as above, we deduce that the

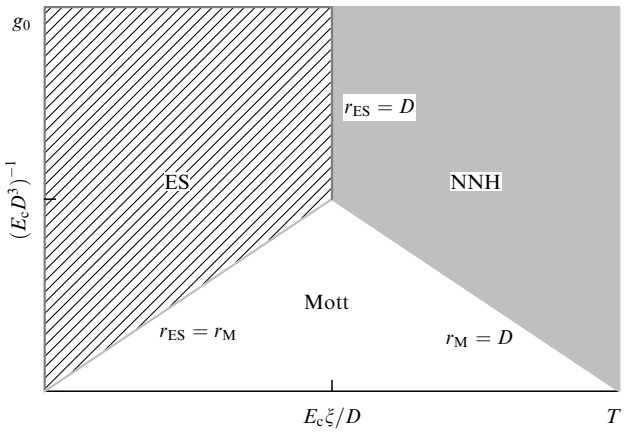

Figure 15. Schematic representation of the experimentally observed types of dependences of the conductivity $G(T)$ for a QD array in different intervals of temperature T and at different densities of states g_0. At low temperatures, transport governed by the ES mechanism, $p = 1/2$, is observed; at small densities of states and intermediate temperatures, transport follows the Mott law, $p = 1/4$. At high temperatures, nearest neighbor hops (NNHs) are observed, $p = 1$. The temperature dependences pass into each other when the typical hopping lengths r_{ES}, r_M become incomparable with each other or with the QD diameter D.

conductivity is given by formula (2) with $p = 1/2$ and $E_0 = E_{ES} \sim e^2/\kappa\xi$. The coefficient in the last relation is determined by percolation theory; for a bulk semiconductor, it is equal to 2.7 [96] and must be the same for a QD array. The typical length of a hop is then $r_{ES} = \xi(E_{ES}/kT)^{1/2}/4$, and the typical energy of the electrons that participate in transport is $\varepsilon_{ES} = (E_{ES}kT)^{1/2}/2$.

In the general case, the $G(T)$ law governing the conductivity of a QD array is determined by the parameters of the array, which we have considered above, and by the temperature interval. As an example, we consider a system with the density of states $g(\varepsilon)$ shown in Fig. 10c. Transport observed in the QD array depending on the temperature T and the density of states g_0 is represented schematically in Fig. 15, as was done in [40].

At low temperatures $kT \ll E_{ES}^2/\varepsilon_M$, long-distance hops occur: $r_{ES} \gg r_M$ in the energy strip $\varepsilon_M \ll \varepsilon_{ES} \ll \Delta_{ES}$. In this energy range, the density of states and the temperature dependence of conductivity are determined by relations (19) and (2) with $p = 1/2$.

At high temperatures, $kT \gg E_{ES}^2/\varepsilon_M$, transition from the ES conductivity to the Mott conductivity occurs. Most of the hops are over the distance $r_M \gg r_{ES}$ in the energy strip $\varepsilon_M \gg \varepsilon_{ES} \gg \Delta_{ES}$. The density of states is constant and the temperature dependence of conductivity is determined by expression (2) with $p = 1/4$.

In both cases, hops are longer than the size of QDs, $r_{ES,M} \gg D$. At high temperatures, $r_{ES,M} \simeq D$, which means that the hops land on neighboring QDs and the conductivity typically has an activation character, $p = 1$ (see Section 6.4 below).

In the subsequent subsections, we describe the properties of conductivity in some interesting structures involving QD arrays.

6.2 Doped QD arrays

The activation dependence of the conductivity of a QD array on temperature was observed for the average number of donors $N \ll 1$ [38] and the activation energy $E_0 = E_c$ (see Fig. 2).

The explanation of the equality $E_0 = E_c$ is quite simple. In the ground state of the system, each electron is on one of just a few QDs that contain a donor, and each QD is then electrically neutral. When such a QD containing a donor is ionized and the electron moves to a distant QD, which does not contain a donor, the electron frees itself from the donor and "performs hops" between the nearest-neighbor QDs. Such electrons are responsible for the overall conductivity of the array. In this ionized state, the system contains pairs of charged QDs: one with a positive donor and the other with a negative electron. Hence, the ionization process requires the energy $2E_c$. In equilibrium, such ionization processes occur at the same rate as inverse recombination processes. Because the recombination rate is proportional to n^2, where n is the concentration of free electrons on empty QDs, then, as a result of equilibration, the activation energy is equal to E_c.

We proceed to the case of strongly doped QDs made of Si and ZnO. For Si (as well as for ZnO), the effective mass is sufficiently large (see the Table) and the ratio $\Delta/E_c \simeq 2 \ll D/\rho$ is small. Therefore, the random Coulomb potential is the main source of disorder in such a system. This corresponds to the lower part of the diagram shown in Fig. 11a, b. We can see from this diagram that, as N increases, the QD array must pass from the OI state to the I state.

In the OI state, when the Fermi level is practically in the middle of the gap Δ between energy shells (for example, 1s and 1p), the density of states is small, and Mott-type conductivity must be observed at experimentally attainable temperatures.

As N increases, the Fermi level coincides in energy with a quantum level (for example, 1p), where the density of states is high. In that case, due to electron–electron correlations, a Coulomb gap forms on the Fermi level, which then leads to transport governed by the ES law.

Thus, as N increases, the transition from Mott-type to ES-type conductivity must be observed simultaneously with a decrease in the resistance of the sample. Just such a transition was observed in [115].

The same argument shows that, in the I state, when the density of states is practically uniform, the conductivity follows the ES law for any N.

In studies of strongly doped Si [21] and ZnO [36], the conductivity was observed to follow the ES law, because the QD array was apparently in the I state. An array of such QDs can never be in the BM state, because that would require the condition $\Delta/E_c > (D/\rho)^{5/3}$ to be satisfied (Fig. 11b), i.e., would require that $D \sim \rho$. We note that in [21], dependence (21) was also derived for ξ. An increase in the thickness of the oxide layer on an Si QD (an increase in s) resulted in a decrease in ξ.

Transport governed by the ES mechanism was also observed in [116, 117], where two-dimensional Ge QD arrays on an Si substrate were investigated, and charge carriers were introduced by creating a boron delta-layer in Si. As a result, the holes were transferred to Ge and the boron delta-layer was charged negatively. At the filling $N \simeq 2$, the localization length ξ sharply decreased. In that case, the ratio Δ/E_c is sufficiently large, and hence the system was in the OI state; characteristic oscillations of the localization length (and also the conductivity) were observed when varying the average number of charges N in the system. However, no Mott transport was observed in the case where the Fermi level was between the 1s and 1p levels of individual particles. We also note that, for large N, the system conductivity obeyed the scaling hypothesis [118].

6.3 Charge distribution in a field transistor

Two types of disorder can be imagined in the structure of a field transistor: in size and in distances between QDs. In [119], the case of arbitrary disorder in size was considered at the temperatures $kT \ll E_c$ such that the conductivity is determined by hops to neighboring QDs. We focus on the case $\Delta \gg E_c \gg \gamma_A \gg t$, which corresponds to low disorder in the system, Δ, $E_c \gg \gamma_A$, when disorder does not play any major role in the distribution of electrons. However, because $\gamma_A \gg t$, disorder is much greater than the overlap integral between neighboring QDs, and the metal–insulator transition is absent.

A property of the system of QDs in a field transistor is that only a small part of the QD array — those QDs that are located directly under the field electrode (Fig. 3b) — participate in conductivity. The thickness of this near-surface domain is actually defined by the screening radius r_0, Eqn (17).

In the first approximation, we can use a simplified approach where the QD array is represented as a conventional bulk semiconductor in the metal–insulator–semiconductor system [32, 120]. If the surface concentration of electrons is n_s, then the characteristic three-dimensional concentration is $n \sim n_s/r_0$. With the density of states $g \sim n/E_F \sim mn^{1/3}/\hbar^2$, we obtain

$$r_s = \left(\frac{225\pi}{8}\right)^{1/5} \frac{a_B}{(n_s a_B^2)^{1/5}} . \tag{28}$$

The numerical coefficient in this expression was found in [121]. With reasonable experimental values of the concentration n_s, we have $r_s \sim a_B \simeq 1$ nm; this means that all the electrons are in the first layer of QDs.

In the above derivation of expression (28), the discreteness of charges and the existence of discrete energy levels were ignored. Taking these two factors into account has shown [119] that, under reasonable parameter values, most of the electrons may be in not one but the first two layers of the QD array, the layers nearest to the gate. Indeed, if we estimate the screening radius using expression (17), then we can consider two cases: $\Delta \ll E_c$ and $\Delta \gg E_c$.

For $\Delta \ll E_c$, the parameter E_c is the only characteristic energy scale in the system, and the density of states at the Fermi level is $g \sim 1/E_c D'^3$; we then obtain $r_0 \simeq D'/2\sqrt{\pi}$. This means that electrons fill only the first layer.

For $\Delta \gg E_c$, the energy Δ gives another characteristic energy scale, and r_0 increases as $D'\sqrt{\Delta}/2\sqrt{\pi}$. However, for realistic values $E_c \ll \Delta \ll 20E_c$, all electrons reside in the first two layers of the QD array. In that case, relation (17) can be used to observe the changes that occur as the number of electrons gradually increases (Fig. 16a). When the number of electrons is small, they fill the 1s level of the first QD layer, and the Fermi level coincides with that level. As the number of electrons increases, the Fermi level lands in the gap between the 1s and 1p levels of the first QD layer, $g = 0$, and the electrons fill the 1s level of the second layer. Upon a further increase in the number of electrons, the Fermi level lands on the 1p level of the first QD layer. The density of states on that level is large, and hence all the electrons return to the first QD layer.

These estimates allow us to restrict the subsequent analysis to the conductivity of only two QD layers, those nearest to the gate.

We let N_1 and N_2 denote the average numbers of electrons in QDs of the first and second layers. They are related to the applied bias on the gate V as

$$N_1 + N_2\left(1 + \frac{D'}{L}\right) = \frac{V\kappa}{4\pi d(e/D'^2)} , \tag{29}$$

where L is the thickness of the gate insulator (Fig. 3b).

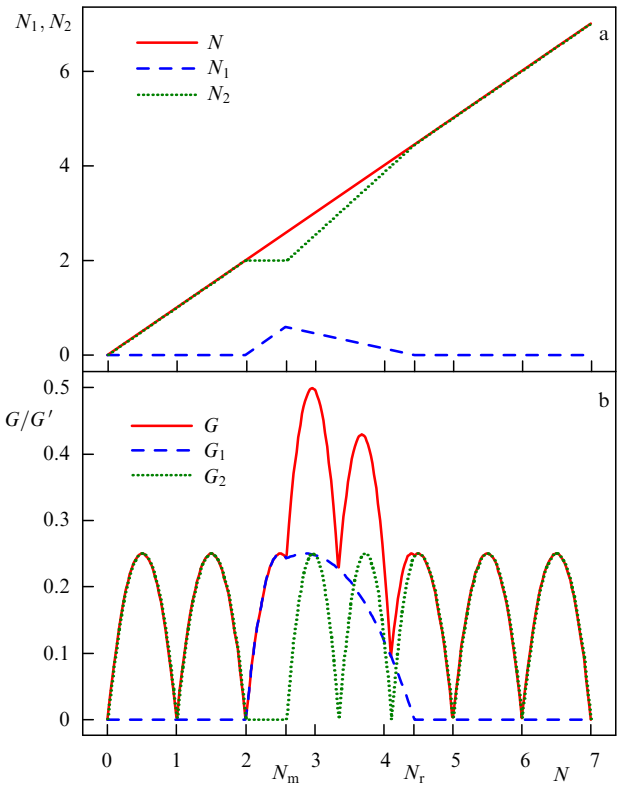

Figure 16. (a) Distribution of electrons between the first and the second layers in a QD array in a field transistor system. $N_{1,2}$ are the average numbers of electrons in the first and the second layers; $N = N_1 + N_2$. For $N < 2$, only the first layer is filled; for $2 < N < N_m$, electrons fill the second layer; and for $N_m < N < N_r$, electrons return from the second layer to the first. (b) Dependences of the conductivities $G_{1,2}$ of the first and second layers, and the total conductivity of a QD array in a field transistor system. It is assumed that $T \ll E_c$, i.e., the processes of electron hopping to a QD with an extra electron are assumed to have a low probability.

In what follows, we discuss the dependence of the conductivity of each layer $G_{1,2}(N)$ and the total conductivity $G(N)$ as functions of $N = N_1 + N_2$. In experiment, conductivity is studied as a function of the bias, and it is therefore useful to give the relation between N and V. For $L \gg D'$, we obtain $N = V\kappa/4\pi L(e/D'^2)$.

To start with, Fig. 16 shows that the second layer is filled only for $N > 2$, in full agreement with the argument adduced above. The second layer starts being filled only when the 1s level of the first QD layer is filled.

Interestingly, for $N > N_r$, all electrons again reside only in the first layer. Indeed, moving an electron under the action of an electric field from the first layer to the second layer requires producing work against the external field, which by the order of magnitude is equal to NE_c. The energy gained is then Δ, because the electron does not go to the 1p level in the first layer. Therefore, for $N > N_r \simeq \Delta/E_c$, all the electrons reside in the first layer. A more detailed calculation shows that

$$N_r = \frac{\Delta/E_c}{(D/D')(2\pi - \alpha) - 2} , \tag{30}$$

where α depends on the lattice type, with $\alpha \simeq 2.37$ for the cubic lattice.

The range $2 < N < N_r$ in which the electrons are located between the two layers exists only for $\Delta > \Delta_c$. In this range of N, the number of electrons in the second layer $N_2 = N - 2$ first increases as long as $2 < N < N_m$, where

$$N_m = \frac{\Delta/E_c + 4 + 2\alpha D/D'}{2\pi D/D'}\,, \tag{31}$$

and then decreases linearly to zero.

The value of Δ_c can be found from the condition that $N_r = 2$:

$$\Delta_c = E_c \frac{D}{D'}(4\pi - 2\alpha) - 4\,. \tag{32}$$

6.4 Disorder in sizes and in distances between QDs

The effect of disorder in the distribution of distances between QDs on the conductivity of a QD array has not been addressed in published papers.

Here, we consider the case of such disorder and simultaneously take disorder in sizes into account similarly to how this was done for metallic particles in [122–124]. We analyze the conductivity G' of a QD array in a field transistor system when the number of electrons is sufficiently small and for high temperatures such that the hops are to the nearest neighbors.

We assume that the distances between QDs are distributed uniformly from zero to s_m, where s_m is the maximum distance between neighboring QDs. We also assume that the spread in energies of electrons from one QD to another due to variation in size is uniform in the range from zero to $2\gamma_A$. There is no difficulty in generalizing the approach considered below to any shape of the distribution.

We right away give the final result for the conductivity of a QD array with the two types of disorder considered:

$$\ln\frac{G'}{G_0} = \begin{cases} -\left(P_c\dfrac{2s_m}{\xi} + \dfrac{1}{2}\dfrac{2\gamma_A}{kT}\right), & T \geqslant T_h \\ -\sqrt{2P_c\dfrac{2s_m}{\xi}\dfrac{2\gamma_A}{kT}}, & T_l \leqslant T \leqslant T_h \\ -\left(P_c\dfrac{2\gamma_A}{kT} + \dfrac{1}{2}\dfrac{2s_m}{\xi}\right), & T \leqslant T_l\,. \end{cases} \tag{33}$$

Here, $G_0 = R_0^{-1}$ is a dimensional factor and P_c is the percolation threshold depending on the type of lattice arrangement of QDs; the values of P_c for various lattices are given in [96]. We restrict ourselves to the approximation $P_c \simeq 2/Z$, where Z is the number of the nearest-neighbor QDs. This approximation means that in percolation each QD must be connected with two neighbors. Expression (33) holds for lattices in which $P_c \leqslant 0.5$, and the results can easily be generalized to other lattices. The temperatures T_h and T_l are determined by the condition that the conductivity is a continuous function of temperature at the points $T = T_h, T_l$:

$$kT_l = \frac{1}{2P_c}2\gamma_A\frac{\xi}{2s_m}\,,$$

$$kT_h = 4P_c\gamma_A\frac{\xi}{2s_m}\,.$$

The dependence of $\ln(G'/G_0)$ on temperature is shown in Fig. 17b.

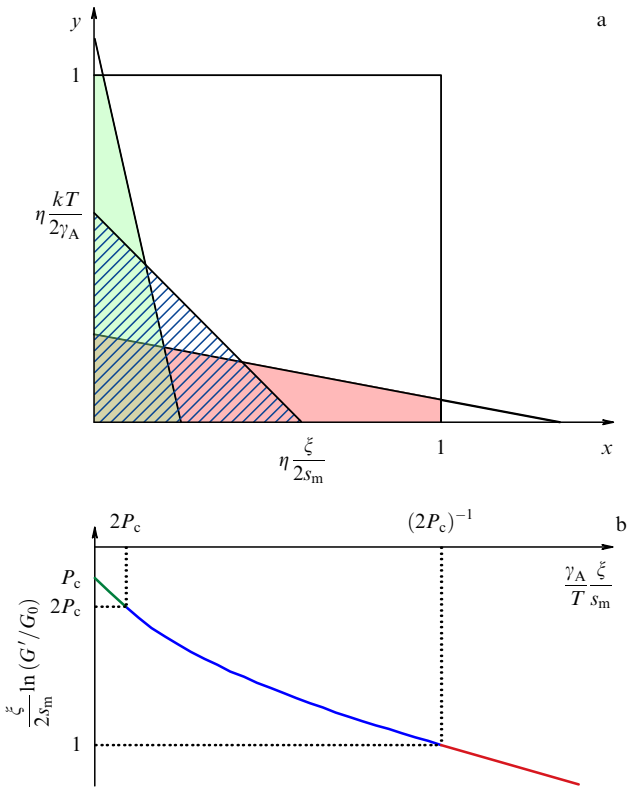

Figure 17. (Color online.) (a) Area of the hatched domain is equal to the probability $P(\eta)$ that the sum of two random variables x, y in (36), distributed uniformly on [0,1], is less than η. (b) Dependence of conductivity G' on temperature T for a QD array with a percolation threshold P_c in the case with disorder in size and in the distance between QDs. It was assumed in the calculations that the distances are distributed uniformly from zero to s_m, where s_m is the maximum distance between neighboring QDs. The spread over electron energies from one QD to another due to size variations is uniform in the range from zero to $2\gamma_A$.

To derive expression (33), we use percolation theory for a network of resistances [96].

We write the resistances R_{ij} between QDs i and j in the form (see (26))

$$R_{ij} = R_0\exp(\eta_{ij})\,, \tag{34}$$

where

$$\eta_{ij} = \frac{2s_m}{\xi}x_{ij} + \frac{2\gamma_A}{kT}y_{ij}\,, \tag{35}$$

with x and y being dimensionless random variables uniformly distributed in the interval $[0, 1]$.

We first consider the case of high temperatures $kT \gg kT_h, \gamma_A$, when the second term in expression (35) can be disregarded, and calculate the conductivity of the system using percolation theory.

We choose η and replace all resistances $\eta_{ij} > \eta$ with infinite resistances, i.e., break the chain. All the resistances with $x_{ij}2s_m/\xi < \eta$ remain in the resistance network. A random resistance is unbroken with the probability $P(\eta) = \eta\xi/2s_m$. In other words, $P(\eta)$ is the probability that the random variable x uniformly distributed in $[0, 1]$ is less than $\eta\xi/2s_m$.

If η is small, then $P(\eta)$ is also small, and the corresponding resistances form isolated clusters. As η increases and reaches a

critical value η_c, an infinite cluster of resistances is formed. At that instant, $P(\eta)$ is equal to the percolation threshold P_c. The critical value η_c is to be found from the condition $P_c = \eta_c \xi / 2s_m$, and for $\gamma_A/k, T_h \ll T$ the corresponding conductivity is given by formula (33) with the term γ_A/kT omitted.

We now consider the intermediate case $T_l \leqslant T \leqslant T_h$, when the terms in (35) have the same order of magnitude. All the resistances with

$$\frac{2s_m}{\xi} x + \frac{2\gamma_A}{kT} y < \eta \tag{36}$$

are part of the network and are not broken. In this case, it is necessary to find the probability $P(\eta)$ that the sum $x(2s_m/\xi) + y(2\gamma_A/kT)$ of two random variables x and y uniformly distributed on $[0, 1]$ is less than η. This means that $P(\eta)$ gives the probability that a random point with coordinates x, y is in the hatched triangle in Fig. 17a. This probability is

$$P(\eta) = \frac{\eta^2}{2(2s_m/\xi)(2\gamma_A/kT)} .$$

We find η_c from the condition $P(\eta_c) = P_c$, and the conductivity of the resistance network with $T_l \leqslant T \leqslant T_h$ is then given by formula (33).

In the case of low temperatures $T \leqslant T_l$, we can have $\eta\xi/2s_m$ greater than unity. Then, $P(\eta)$ is the probability that a random point with coordinates x, y is in the trapezoid domain shown in green in Fig. 17a.

This probability is

$$P(\eta) = \frac{1}{4} \frac{kT}{\gamma_A} \left(2\eta - \frac{2s_m}{\xi} \right),$$

and therefore the conductivity of the resistance network for $T < T_l$ is given by formula (33).

The same approach can also be applied to high temperatures $T > T_h$. We then eventually arrive at expression (33).

It follows from (33) that, even for activation transport, when hops are performed to the nearest neighbors, the temperature dependence of the conductivity is determined by expression (2) with $p \neq 1$. At much lower temperatures $kT \ll \gamma_A$, the possibility of electron hopping over one, two, or more QDs must be taken into account. Eventually, this leads to the Mott transport or the ES transport if electron–electron correlations are taken into account.

The main drawback of the above argument is that the distribution of inter-QD distances in the array has not been found either experimentally or theoretically. The distances between QDs are largely determined by the interaction of ligands on QD surfaces. Although the problem of a random packing of hard spheres was solved quite long ago [125], the packings of spheres covered with "springs" have not been investigated. Using distributions of distances in a QD array, we can obtain any dependence of the conductivity on temperature in the range $T_l \leqslant T \leqslant T_h$.

6.5 Conductivity in a field transistor

As we have already noted, the dependences $N_1(N)$ and $N_2(N)$ are nonmonotonic in a QD array, which leads to a nonmonotonic dependence of the conductivity (Fig. 16b). We consider the conductivity in the case of relatively high temperatures $\gamma_A \ll kT \ll E_c, \Delta$, when hops to the neighboring QDs dominate, but the probability of hopping to the QDs occupied with electrons is low.

As can be seen from numerical computations by the Kirchhoff method in [119], the conductivity of an entire QD array is equal to the sum of conductivities of the participating layers, which can be calculated independently of each other if the filling numbers are known: $G = G_1(N_1) + G_2(N_2)$. This result can be understood as follows: the conductivity between all pairs of neighboring QDs in a given layer is the same. Accordingly, the same constant gradient of the electrochemical potential along the layer exists, and no electron transport between two QD layers occurs. The situation is very similar to a balanced bridge circuit.

We consider the first layer with $0 < N_1 < 1$. Each QD contains an electron with the probability N_1 and does not contain an electron with the probability $1 - N_1$. The probability of hopping to a neighboring QD that already has an electron is proportional to $\exp(-E_c/kT) \ll 1$, and this hopping can therefore be ignored. This means that only hops between occupied and unoccupied neighboring QDs make a contribution to the conductivity. Therefore, the conductivity is proportional to the number of occupied and unoccupied QDs: $G_1(N_1) = G' N_1(1 - N_1)$. The temperature dependence of the conductivity G' is discussed in Section 6.4.

For $1 < N_1 < 2$, all the QDs contain at least one electron, and only some contain two electrons. Only that second electron travels between QDs. Repeating this argument, we can conclude that $G_1(N_1) = G'(N_1 - 1)(2 - N_1)$. Repeating the argument for $N_1 > 2$ and also for the second layer, we can calculate the conductivity of a system of QDs, which is shown in Fig. 16b.

Taking the disorder in sizes into account [119] makes no major changes to the results, the qualitative picture being preserved up to $\gamma_A \simeq E_c$. The difference is only that, for $N = 1, 3, 4 \ldots$, the conductivity does not go to zero as shown in Fig. 16b but just slightly decreases.

In [126], the Monte Carlo method was used to consider a bulk array of QDs in which the average number of electrons N was fixed. Disorder in sizes was taken into account, and the tunneling coefficient between QDs was calculated. The above analysis is qualitatively applicable to that case as well: the conductivity in a QD array changes periodically as the average number N of electrons in the QDs increases.

We next discuss experimental data for QD arrays in which electrons are induced by the field effect.

From the analysis at the beginning of this section, we can see that, in the absence of disorder, the activation dependence of the conductivity on temperature must be observed at integer values $N = 1, 3, 4 \ldots$ with the activation energy $E_0 = E_c$ and $E_0 = \Delta$ for $N = 2$. The activation dependence can be observed due to disorder in sizes, in which case $E_0 = \gamma_A$ (see Section 6.4) or, similarly to the case of weakly doped arrays (see Section 6.2), due to uncontrolled impurity donors. We must bear in mind that attaining high filling numbers $N > 2$ in a field transistor is a practically infeasible task, because the gate bias V_g must then be too high.

In experimental work [127], a field transistor with PbSe QDs was investigated. At small V_g, most of the holes occurred in the array as a result of activation with uncontrolled acceptors ε_A, and, due to size disorder, the holes had to overcome the energy spread γ_A from one QD to another. As a result, the activation energy turned out to be equal to the sum of these two energies: $E_0 \simeq \varepsilon_A + \gamma_A$. As V_g decreased, the holes filled the 1s level of the first QD layer. The activation

energy then decreased, because the holes did not have to be activated with acceptors: $E_0 \simeq \gamma_A$.

The effect of ligands on transport was also studied experimentally in similar PbS QDs [128]. A similar dependence of E_0 on V_g was observed when the QDs were covered with the same ligands as in the case of PbSe. Replacing the ligands with shorter ones, the Mott mechanism of electron conductivity could be observed at low temperatures, with the hops occurring over the area formed by the acceptors. A reduction in s leads to an increase in ξ, and hops to more distant neighbors become possible. In that case, the Mott type of conductivity can be explained by the fact that the dielectric permittivity of QDs is large ($\kappa_{QD} \simeq 170$), and, hence, the dielectric permittivity κ of the array is also large. This suppresses Coulomb effects, and ES transport can be observed only at very low temperatures.

We note an unresolved contradiction between [127, 128] and paper [129], where, in the same temperature range, the ES transport was observed in a field transistor with PbSe QDs covered with long ligands.

An important characteristic of a field transistor is the mobility of charges, which for real $N \ll 1$ is determined by the ratio G'/en. By the order of magnitude, the maximum mobility in such structures is 10 $cm^2\ V^{-1}\ s^{-1}$ [32, 59, 130]. It is worth recalling here that mobility depends on the distance s between QDs exponentially, as was experimentally demonstrated in [130], where the length of ligands covering the particles was measured.

At small filling numbers N, transport in QD arrays can be studied by exploring the dynamics of photoexcited electrons by measuring the diffusion coefficient [103, 131] and subsequently calculating the mobility. It turns out that, by the order of magnitude, the mobility of such electrons in a QD array is 10^{-1} $cm^2\ V^{-1}\ s^{-1}$ [132], which agrees with typical mobility values in QD arrays [130]. We note that the dynamics of photoexcited electrons can be significantly affected not only by disorder in sizes but also by disorder in inter-QD distances [133].

6.6 Doping from the surface

We now describe the properties of transport in a QD array where electrons are induced by an ionic liquid. As was noted in Section 2, inducing the electrons this way is similar to doping from the surface of each QD (Fig. 3c), but there are two differences. The first is that the Coulomb potential of all ions in the ionic liquid creates additional disorder in the system, as was shown experimentally with the example of a bulk semiconductor [134]. However, we can expect this effect to be fairly weak and disregard it.

The second difference is that the temperatures at which the liquid solidifies can be comparable with the Coulomb potential γ_S in the system, which leads to correlations in positions of ions. These correlations diminish the role of Coulomb disorder and enhance the role of geometric disorder [82, 93]. In particular, in the diagram in Fig. 11 for $\alpha(D/\rho)^2 \gg 1$, the parameter domain where the OI state exists widens, and the parameter domain where the I state exists narrows. For $\alpha(D/\rho)^2 \ll 1$, both domains become narrower, and only the BM state persists.

In [40, 135], the conductivity of a QD array was investigated experimentally at high concentrations of electrons $N \lesssim 6$ (see Fig. 2). Overall, the obtained data agree with the diagrams in Figs 11 and 12. The QD array is in the OI state, where the density of states is periodic in energy and the maxima coincide with the 1s and 1p levels of an individual QD. When the Fermi level coincides with these maxima, $N \neq 2$, transport obeys the ES law (see Fig. 2, the case $p = 1/2$); otherwise, for $N \simeq 2$, the Fermi level is in the middle of the gap between the 1s and 1p levels, where the density of states is minimal and transport following the Mott law is observed (see Fig. 2, the case $p = 1/4$). We note that the localization length is then minimal, as follows from the diagram in Fig. 12.

Finally, for small concentrations $N \simeq 1$, as well as in the considered case of a doped QD array, activation transport was observed in [136]. The activation energy was $E_0 = E_c$ and changed inversely proportionally to the particle diameter D. This follows from formula (4).

There are two reports [39, 61] on experiments in which a nontypical dependence of the conductivity on temperature with $p = 2/3$ was observed in a QD array (see Fig. 2, the case $p = 2/3$). The mechanisms of its appearance are unknown. This dependence manifests itself when inducing electrons with an ionic liquid [61] or in doping from the surface at relatively low temperatures [39]. In other words, such dependence is observed in those cases where repulsion between donors can be important. Because the $p = 2/3$ dependence is observed for conductivity ranging over five orders of magnitude, it can hardly be explained by a crossover between the ES dependence at low temperatures ($p = 1/2$) and activation transport at high temperatures ($p = 1$). In addition, this dependence is observed at a quite high conductivity of films. In attempting to approximate these experimental data with the ES dependence, we obtain a localization length ξ that greatly exceeds the size D of the particles. This means that the QD array is in the vicinity of the metal–insulator transition. Possibly, the appearance of this dependence is an interesting feature of QD arrays near the metal–insulator transition with correlated donors.

7. Conclusions

The physical properties of QD arrays have been actively investigated over the last decade, which has much to do with the possibility of varying the optical properties by changing the sizes. However, detailed studies of the electron conductivity mechanisms have received less attention. In this review, we offer a systematic theoretical description of conductivity mechanisms in QD arrays. The main parameters characterizing such arrays were discussed in sufficient detail. We have discussed disorder in QDs due to differences in size, distance, and the number of donors. We also considered the effect of disorder on the metal–insulator transition and on electron transport in the insulating phase.

We have shown that QD arrays are essentially different from metallic QD arrays due to the quantum confinement effect, which turns out to be more significant compared with the Coulomb blockade effect. Moreover, the number of electrons in such QDs varies in a wide range as the result of disorder in the number of donors in a QD, which is not the case for metallic nanoparticles. In a certain sense, a QD system is similar to a system of nanoparticles made of different metals with different values of the work function. An important topic of this review was the description of microscopic quantities, such as the localization length ξ, the overlap integral t, and the density of states $g(\varepsilon)$. This allowed describing the metal–insulator transition and the electron transport in the insulating phase in greater detail than for a

system of metallic nanoparticles. The strategies to calculate these quantities — developed in this review — can also be used for metallic nanoparticles.

We have shown how the conductivity theory of bulk semiconductors can be modified so as to describe electron transport in QD arrays. All the principal theoretical conclusions are compared with experimental results for transport in QD arrays. This comparison shows that the theoretical approaches developed in recent years, including those in [21, 82], explain well the regularities observed in the conductivity of QD arrays.

We must note that theoretical descriptions of the electron transport mechanism in bulk semiconductors or in an array of metallic nanoparticles constitute a coherent and finished landscape. This is currently not the case with the electron transport mechanism in arrays of semiconducting QDs, where a number of questions remain unanswered. In particular, theoretical analysis is needed to explain the observed linear dependence of magnetoresistance for strongly doped QDs [137] and features of noise such as the inversely proportional dependence of the Hooge constant on the conductivity [138]. Also, electron transport in a QD array is strongly influenced by surface states [8], but theoretical analysis of this influence has not been given sufficient attention.

We also note that the distribution over inter-QD distances can substantially change the character of electron transport, as we saw in Section 6.4. Even at high temperatures, the temperature dependence of conductivity can be given by expression (2) with $p \neq 1$. Unfortunately, there are no experimental data on a detailed study of the packing of QDs into an array, and the distribution of distances between QDs is unknown.

The occurrence of dependence (2) with $p = 2/3$ in a QD array remains enigmatic (see Section 6.6). This is all the more surprising because this dependence manifests itself in the vicinity of the insulator–metal transition when, apparently, the system must follow the scaling law.

Further development of the theory expounded in this review leads to the question of approaches to the theoretical description of transport of other quasiparticles in QD arrays, for example, excitons [139–142].

We believe that the problems listed here can be solved based on a theory whose main ingredients are the approaches described in this review.

Acknowledgments

The author has the pleasant duty to express his gratitude to B I Shklovskii, with whom constant discussions resulted in the appearance of this review, A Ya Vul for support over many years, N S Averkiev, who initiated this work, and P I Arseev for the discussions and useful suggestions.

References

1. Kagan C R et al. *Science* **353** aac5523 (2016)
2. Pi X D et al. *Nanotechnology* **19** 245603 (2008)
3. Ekimov A I, Onushchenko A A, Tsekhomskii V A *Fiz. Khim. Stekla* **6** 511 (1980)
4. Rossetti R, Nakahara S, Brus L E *J. Chem. Phys.* **79** 1086 (1983)
5. Efros Al L, Efros A L *Sov. Phys. Semicond.* **16** 772 (1982); *Fiz. Tekh. Poluprovodn.* **16** 1209 (1982)
6. Chuang C-H M et al. *Nat. Mater.* **13** 796 (2014)
7. Sun L et al. *Nat. Nanotechnol.* **7** 369 (2012)
8. Pal B N et al. *Adv. Funct. Mater.* **22** 1741 (2012)
9. Kairdolf B A et al. *Annu. Rev. Anal. Chem.* **6** 143 (2013)
10. Keuleyan S et al. *Nature Photon.* **5** 489 (2011)
11. Jeong K S, Guyot-Sionnest P *ACS Nano* **10** 2225 (2016)
12. Razumov V F *Phys. Usp.* **59** 1258 (2016); *Usp. Fiz. Nauk* **186** 1368 (2016)
13. Efros Al L, Rosen M *Annu. Rev. Mater. Sci.* **30** 475 (2000)
14. Klimov V I *Annu. Rev. Phys. Chem.* **58** 635 (2007)
15. Shirasaki Y et al. *Nat. Photon.* **7** 13 (2013)
16. Lan X, Masala S, Sargent E H *Nat. Mater.* **13** 233 (2014)
17. Averin D V, Likharev K K *J. Low Temp. Phys.* **62** 345 (1986)
18. van der Wiel W G et al. *Rev. Mod. Phys.* **75** 1 (2002)
19. Beloborodov I S et al. *Rev. Mod. Phys.* **79** 469 (2007)
20. Zabet-Khosousi A, Dhirani A-A *Chem. Rev.* **108** 4072 (2008)
21. Chen T et al. *Nat. Mater.* **15** 299 (2016)
22. Kagan C R, Murray C B *Nat. Nanotechnol.* **10** 1013 (2015)
23. Zhu J, Hersam M C *Adv. Mater.* **29** 1603895 (2017)
24. Kagan C R *Chem. Soc. Rev.* **48** 1626 (2019)
25. Kim J-Y, Kotov N A *Chem. Mater.* **26** 134 (2014)
26. Whitham K et al. *Nat. Mater.* **15** 557 (2016)
27. Treml B E et al. *ACS Appl. Mater. Interfaces* **9** 13500 (2017)
28. Ondry J C, Hauwiller M R, Alivisatos A P *ACS Nano* **12** 3178 (2018)
29. Norris D J, Efros Al L, Erwin S C *Science* **319** 1776 (2008)
30. Choi J-H et al. *Science* **352** 205 (2016)
31. Jang J et al. *Nano Lett.* **15** 6309 (2015)
32. Liu Y et al. *Nano Lett.* **13** 1578 (2013)
33. Yu D, Wang C, Guyot-Sionnest P *Science* **300** 1277 (2003)
34. Guyot-Sionnest P *J. Phys. Chem. Lett.* **3** 1169 (2012)
35. Edwards P P, Ramakrishnan T V, Rao C N R *J. Phys. Chem.* **99** 5228 (1995)
36. Greenberg B L et al. *Nano Lett.* **17** 4634 (2017)
37. Moreira H et al. *Phys. Rev. Lett.* **107** 176803 (2011)
38. Chen T et al. *J. Phys. Chem. C* **118** 19580 (2014)
39. Turk M E et al. *Nano Lett.* **14** 5948 (2014)
40. Liu H, Pourret A, Guyot-Sionnest P *ACS Nano* **4** 5211 (2010)
41. Nelson J et al. *Phys. Rev. B* **92** 085424 (2015)
42. Shklyaev A A, Ichikawa M *Phys. Usp.* **51** 133 (2008); *Usp. Fiz. Nauk* **178** 139 (2008)
43. Ledentsov N N et al. *Phys. Usp.* **39** 393 (1996); *Usp. Fiz. Nauk* **166** 423 (1996)
44. Boles M A, Engel M, Talapin D V *Chem. Rev.* **116** 11220 (2016)
45. Murray C B, Kagan C R, Bawendi M G *Annu. Rev. Mater. Sci.* **30** 545 (2000)
46. Talapin D V et al. *Chem. Rev.* **110** 389 (2010)
47. Shim M, Guyot-Sionnest P *Nature* **407** 981 (2000)
48. Talapin D V, Murray C B *Science* **310** 86 (2005)
49. Makkar M, Viswanatha R *RSC Adv.* **8** 223 (2018)
50. Kortshagen U R et al. *Chem. Rev.* **116** 11061 (2016)
51. Greenberg B L et al. *Nano Lett.* **15** 8162 (2015)
52. Moroz P et al. *ACS Nano* **7** 6964 (2013)
53. Ip A H et al. *Nat. Nanotechnol.* **7** 577 (2012)
54. Nagaoka Y et al. *Nature* **561** 378 (2018)
55. Urban J J et al. *J. Am. Chem. Soc.* **128** 3248 (2006)
56. Baumgardner W J, Whitham K, Hanrath T *Nano Lett.* **13** 3225 (2013)
57. Kalesaki E et al. *Phys. Rev. B* **88** 115431 (2013)
58. Sandeep C S S et al. *ACS Nano* **8** 11499 (2014)
59. Choi J-H et al. *Nano Lett.* **12** 2631 (2012)
60. Goldman A M *Annu. Rev. Mater. Res.* **44** 45 (2014)
61. Houtepen A J, Kockmann D, Vanmaekelbergh D *Nano Lett.* **8** 3516 (2008)
62. Martinez B et al. *ACS Appl. Mater. Interfaces* **9** 36173 (2017)
63. Meir Y, Wingreen N S, Lee P A *Phys. Rev. Lett.* **66** 3048 (1991)
64. Wang L W, Zunger A *Phys. Rev. Lett.* **73** 1039 (1994)
65. Delerue C, Lannoo M, Allan G *Phys. Rev. B* **68** 115411 (2003)
66. Madelung O *Semiconductors: Data Handbook* (Berlin: Springer, 2013)
67. Ekimov A I et al. *J. Luminescence* **46** 83 (1990)
68. Feigel'man M V, Ioselevich A S *JETP Lett.* **81** 277 (2005); *Pis'ma Zh. Eksp. Teor. Fiz.* **81** 341 (2005)
69. Landauer R *AIP Conf. Proc.* **40** 2 (1978)

70. Landau L D, Lifshitz E M *Electrodynamics of Continuous Media* (Oxford: Butterworth-Heinemann, 1980); Translated from Russian: *Elektrodinamika Sploshnykh Sred* (Moscow: Fizmatlit, 2004)
71. Reich K V, Shklovskii B I *Appl. Phys. Lett.* **108** 113104 (2016)
72. Sareni B et al. *J. Appl. Phys.* **80** 1688 (1996)
73. Shen L C et al. *J. Appl. Phys.* **67** 7071 (1990)
74. Reich K V, Shklovskii B I *ACS Nano* **10** 10267 (2016)
75. Lord Rayleigh F R S *Philos. Mag. 5* **43** 259 (1897)
76. Bethe H A *Phys. Rev.* **66** 163 (1944)
77. Levine H, Schwinger J *Phys. Rev.* **74** 958 (1948)
78. Gor'kov L P, Pitaevskii L P *Sov. Phys. Dokl.* **8** 788 (1964); *Dokl. Akad. Nauk SSSR* **151** 822 (1963)
79. Herring C, Flicker M *Phys. Rev.* **134** A362 (1964)
80. Landau L D, Lifshitz E M *Quantum Mechanics: Non-Relativistic Theory* (Oxford: Butterworth-Heinemann, 1977); Translated from Russian: *Kvantovaya Mekhanika: Nerelyativistskaya Teoriya* (Moscow: Fizmatlit, 2004)
81. Bardeen J *Phys. Rev. Lett.* **6** 57 (1961)
82. Fu H, Reich K V, Shklovskii B I *Phys. Rev. B* **93** 125430 (2016)
83. Shabaev A, Efros Al L, Efros A L *Nano Lett.* **13** 5454 (2013)
84. Kalesaki E et al. *Phys. Rev. X* **4** 011010 (2014)
85. Tadjine A, Delerue C *Phys. Chem. Chem. Phys.* **20** 8177 (2018)
86. Murray C B, Norris D J, Bawendi M G *J. Am. Chem. Soc.* **115** 8706 (1993)
87. Savitzky B H et al. *Nano Lett.* **16** 5714 (2016)
88. Lifshitz I M *Sov. Phys. Usp.* **7** 549 (1965); *Usp. Fiz. Nauk* **83** 617 (1964)
89. Klimov V I *Science* **287** 1011 (2000)
90. Reich K V et al. *Phys. Rev. B* **88** 245311 (2013)
91. Bae W K et al. *Nat. Commun.* **4** 2661 (2013)
92. Zhang J, Shklovskii B I *Phys. Rev. B* **70** 115317 (2004)
93. Skinner B, Chen T, Shklovskii B I *Phys. Rev. B* **85** 205316 (2012)
94. Tadjine A, Delerue C *Phys. Rev. B* **98** 125412 (2018)
95. Dolgopolov V T *Phys. Usp.* **57** 105 (2014); *Usp. Fiz. Nauk* **184** 113 (2014)
96. Shklovskii B I, Efros A L *Electronic Properties of Doped Semiconductors* (Berlin: Springer-Verlag, 1984)
97. Averin D V, Nazarov Yu V *Phys. Rev. Lett.* **65** 2446 (1990)
98. Beloborodov I S, Lopatin A V, Vinokur V M *Phys. Rev. B* **72** 125121 (2005)
99. Tran T B et al. *Phys. Rev. Lett.* **95** 076806 (2005)
100. Scheele M *Z. Phys. Chem.* **229** 167 (2015)
101. Yang J, Wise F W *J. Phys. Chem. C* **119** 3338 (2015)
102. Lee J S et al. *Nat. Nanotechnol.* **6** 348 (2011)
103. Gilmore R H et al. *ACS Nano* **12** 7741 (2018)
104. Mott N F *Rev. Mod. Phys.* **40** 677 (1968)
105. Sharvin Yu V *JETP* **21** 655 (1965); *Zh. Eksp. Teor. Fiz.* **48** 984 (1965)
106. Matveev K A *Phys. Rev. B* **51** 1743 (1995)
107. Nazarov Yu V, Blanter Ya M *Quantum Transport: Introduction to Nanoscience* (Cambridge: Cambridge Univ. Press, 2009)
108. Gantmakher V F, Dolgopolov V T *Phys. Usp.* **51** 3 (2008); *Usp. Fiz. Nauk* **178** 3 (2008)
109. Lanigan D, Thimsen E *ACS Nano* **10** 6744 (2016)
110. Bogdanovich S, Sarachik M P, Bhatt R N *Phys. Rev. Lett.* **82** 137 (1999)
111. Lee M et al. *Phys. Rev. B* **60** 1582 (1999)
112. Greenberg B L et al. *Sci. Adv.* **5** 1462 (2019)
113. Miller A, Abrahams E *Phys. Rev.* **120** 745 (1960)
114. Chen Q, Guest J R, Thimsen E *J. Phys. Chem. C* **121** 15619 (2017)
115. Benton B T et al. *Nanotechnology* **29** 415202 (2018)
116. Yakimov A I et al. *JETP Lett.* **77** 376 (2003); *Pis'ma Zh. Eksp. Teor. Fiz.* **77** 445 (2003)
117. Yakimov A I et al. *JETP Lett.* **78** 241 (2003); *Pis'ma Zh. Eksp. Teor. Fiz.* **78** 276 (2003)
118. Stepina N P et al. *Phys. Rev. B* **80** 125308 (2009)
119. Reich K V, Chen T, Shklovskii B I *Phys. Rev. B* **89** 235303 (2014)
120. Hetsch F et al. *Mater. Today* **16** 312 (2013)
121. Reich K V, Schecter M, Shklovskii B I *Phys. Rev. B* **91** 115303 (2015)
122. Müller K-H, Yajadda M M A *J. Appl. Phys.* **111** 123705 (2012)
123. Müller K-H et al. *Phys. Rev. B* **66** 075417 (2002)
124. Šimánek E *Solid State Commun.* **40** 1021 (1981)
125. Scott G G D *Nature* **194** 956 (1962)
126. Chandler R E et al. *Phys. Rev. B* **75** 085325 (2007)
127. Mentzel T S et al. *Phys. Rev. B* **77** 075316 (2008)
128. Ray N et al. *Nano Lett.* **15** 4401 (2015)
129. Romero H E, Drndic M *Phys. Rev. Lett.* **95** 156801 (2005)
130. Liu Y et al. *Nano Lett.* **10** 1960 (2010)
131. Zhitomirsky D et al. *ACS Nano* **7** 5282 (2013)
132. Proppe A H et al. *Nano Lett.* **18** 7052 (2018)
133. Gilmore R H et al. *Nano Lett.* **17** 893 (2017)
134. Petach T A et al. *ACS Nano* **11** 8395 (2017)
135. Yu D et al. *Phys. Rev. Lett.* **92** 216802 (2004)
136. Kang M S et al. *Nano Lett.* **10** 3727 (2010)
137. Liu H, Guyot-Sionnest P *J. Phys. Chem. C* **119** 14797 (2015)
138. Liu H, Lhuillier E, Guyot-Sionnest P *J. Appl. Phys.* **115** 154309 (2014)
139. Kholmicheva N et al. *ACS Energy Lett.* **2** 154 (2016)
140. Moroz P, Romero L R, Zamkov M *Chem. Commun.* **55** 3033 (2019)
141. Chen W et al. *J. Phys. Chem. Lett.* **10** 2058 (2019)
142. Azzaro M S et al. *Nano Lett.* **18** 3259 (2018)